The lncRNA landscape of cardiac resident macrophages and identification of *Schlafenlnc* as a regulator of macrophage migratory function

Anne Dueck[1,2], Lara Althaus[1,2], Kathrin Heise[1,2], Dena Esfandyari[1,2], Seren Baygün[3], Ralf P. Brandes[4,5], Julien Gagneur[2,6,7,8], Nicolas Jaé[5,9], Percy Knolle[10], Matthias S. Leisegang[4,5], Lars Maegdefessel[2,11], Thomas Meitinger[2,7], Niklas Petzold[1,2], Deepak Ramanujam[1,2], Hendrik Sager[2,12], Christian Schulz[2,13], Evangelos Theodorakis[2,6,7,8], Anna Uzonyi[1], Tobias Weinberger[2,13], Michael Bader[14], Marc Schmidt-Supprian[3], Stefan Engelhardt[1,2]

[1] Institute of Pharmacology and Toxicology, Technical University Munich, Munich, Germany
[2] DZHK (German Centre for Cardiovascular Research), partner site Munich Heart Alliance, Munich, Germany
[3] Institute of Experimental Hematology, Central Institute for Translation Cancer Research, School of Medicine, Technical University Munich, Munich, Germany
[4] Institute for Cardiovascular Physiology, Goethe University, Frankfurt, Germany
[5] DZHK (German Centre for Cardiovascular Research), partner site RheinMain, Frankfurt, Germany
[6] Institute of Informatics, Technical University Munich, Munich, Germany
[7] Institute of Human Genetics, Klinikum rechts der Isar, School of Medicine, Technical University of Munich, Munich, Germany
[8] Computational Health Center, Helmholtz Center Munich, Neuherberg, Germany
[9] Institute for Cardiovascular Regeneration, Goethe University Frankfurt, Frankfurt am Main, Germany
[10] Institute for Molecular Immunology, MRI, Technical University Munich, Munich, Germany
[11] Department of Vascular and Endovascular Surgery, Technical University Munich, Munich, Germany
[12] Department of Cardiology, German Heart Centre Munich, Technical University Munich, Munich, Germany
[13] Medizinische Klinik und Poliklinik I, Klinikum der Universität München, Ludwig-Maximilians-Universität, Munich, Germany
[14] Max-Delbrück-Center for Molecular Medicine (MDC), Berlin, Germany

Present address: Anna Uzonyi, Department of Molecular Genetics, Weizmann Institute of Science, Rehovot, Israel

Keywords: long non-coding RNA, cardiac resident macrophages, pressure overload, *Schlafenlnc*, single cell sequencing

ABSTRACT

Cardiac resident macrophages (crMPs) were recently shown to exert pivotal functions in cardiac homeostasis and disease, but the underlying molecular mechanisms are largely unclear. Long non-coding RNAs (lncRNAs) are increasingly recognized as important regulatory molecules in a number of cell types, but neither the identity nor the molecular mechanisms of lncRNAs in crMPs are known. Here, we have employed deep RNA-seq and single cell RNA sequencing to resolve the crMP lncRNA landscape from healthy and diseased murine myocardium. CrMPs express previously unknown and highly cell type-specific lncRNAs, among which one lncRNA, termed *Schlafenlnc*, was particularly abundant and enriched in crMPs. We found *Schlafenlnc* to be necessary for migration-associated gene expression in macrophages *in vitro* and *in vivo* and essential for their adhesion and migration. Collectively, our data provide a basis to the systematic characterization of lncRNAs in crMPs and establish *Schlafenlnc* as a critical regulator of macrophage migratory functions.

INTRODUCTION

Long non-coding RNAs (lncRNAs) are the largest group of non-coding RNA molecules, with 14,764 lncRNA genes currently annotated in mouse and 19,933 in humans (Gencode in October 2022). Although only a small fraction of these has been functionally characterized, there is strong evidence that lncRNAs, through a variety of mechanisms, adopt critical roles in disease, for example in cancer [1], metabolic, neurologic [2] and cardiovascular disease [3]. Macrophage lncRNAs in cardiovascular disease have been primarily characterized in the vasculature and within the context of atherosclerosis, e.g., formation of foam cells or polarization (reviewed in [4]). With regard to cardiac disease, the analysis of lncRNAs and their functions has largely focused on cardiomyocytes [5], endothelial cells [6] and fibroblasts [7] (reviewed in [3]). By contrast, very little is known about lncRNAs in cardiac resident macrophages (crMPs), although this cell type constitutes the largest population of immune cells in the myocardium during homeostasis and also determines cardiac disease processes (reviewed in [8]). CrMPs have in recent years been characterized with respect to their developmental origin [9,10], their composition [10,11] and their putative functions such as roles in cardiac conduction [12,13], hypertrophy [14] or lymph vessel growth [15]. Although it can be readily assumed that many of these functions are subject to lncRNA-mediated regulation, a comprehensive description of the lncRNome from crMPs or functional data on a crMP-specific lncRNA is missing thus far.

In this study, we established the first comprehensive analysis of the lncRNA portfolios of the major cardiac cell types in health and disease, with particular emphasis on macrophages. In mouse myocardium, we identified lncRNAs that are specific for, and define, this cell type. One crMP lncRNA that has previously not been analyzed and which we termed *Schlafenlnc*, stands out for its strong enrichment and high abundance in crMPs. Upon functional characterization of a *Schlafenlnc* knockout in a mouse model for left ventricular pressure overload, we found that this lncRNA regulates macrophage abundance in the heart and the ability of this cell type to exert chemotactic migration. We therefore propose that *Schlafenlnc* critically regulates the function of cardiac macrophages in disease.

RESULTS

lncRNAs are important determinants for the definition of specific cell types

To determine the long non-coding RNA (lncRNA) repertoire in the major cardiac cell types and its changes under disease conditions, we subjected mice to chronic left ventrivcular pressure overload (induced by transverse aortic constriction, TAC), an established model of cardiac inflammation that leads into hypertrophic and fibrotioc remodelling of the heart. At day 6 after surgery, we sacrificed the mice, isolated primary cells by Langendorff digestion [16], and performed droplet-based single cell RNA sequencing (scRNA-seq, Chromium platform) (Fig. 1A). This experimental approach analyzes all cardiac non-myocytes, while the number of cardiac myocytes is decreased due to size constraints of the method. Unsupervised clustering of both samples based on the expression of both coding and non-coding RNAs with the Seurat analysis tool (Seurat V3.2 [17], Gencode vM22 [18]) yielded a total of 20,010 cells after quality control. These comprised all major non-myocyte cardiac cell types (Seurat clustering resolution 0.3, Fig. 1B), including subpopulations of immune cells, fibroblasts, endothelial cells and mural cells (Fig. 1B). Differential gene expression analysis from these cell types revealed distinct sets of protein-coding genes that define each major cardiac cell type as individual clusters (Extended Data Fig. S1), in line with previous reports [19,20].

Despite the generally lower expression levels of lncRNAs in comparison to protein-coding genes [21–24], we were able to readily detect over 440 lncRNAs. Several of the most strongly expressed lncRNAs exhibited a very high level of cell type specificity (Fig. 1C and 1D), suggesting that cardiac cell types can be defined based on their lncRNA transcriptomes. As Fig. 1D shows, our data not only confirmed the previously reported expression of *Meg3* in fibroblasts [25], *H19* in endothelial cells [26] and *Mhrt* in cardiac myocytes [27], but also revealed lncRNAs that had hitherto not been reported to be cell type-specific in the heart. These lncRNAs may reasonably be presumed to potentially exert important roles in their specific cell type, prompting for functional characterization.

To validate the contribution of lncRNAs to cell type identity, we performed differential clustering of the scRNA-seq data sets with or without lncRNA genes, and tested for clustering precision. Independent of whether the top 3,000 variable genes defined by the Seurat pipeline, all annotated genes (n=55,487) or expressed genes (n=19,719, expression value >0) were used to perform clustering, the inclusion of lncRNA marker genes significantly improved clustering compared to protein coding genes alone (Fig. 1E-G). Compared to clustering based on protein-coding genes alone, this resulted in an overall increased sensitivity (indicated by an increased adjusted Rand Index value) and yielded additional subclusters of cell types. Specifically, the detection of clusters representing venous capillary endothelial cells, pericytes, Fabp4^{+} macrophages and Notch2^{+} fibroblasts was dependent on the inclusion of lncRNAs (resolution 0.65) (Fig. 1H, Extended Data Fig. S1B).

In conclusion, lncRNAs were shown to be a valuable determinant of defining clusters and fine-tuning cell type assignations.

As a means to approach lncRNAs of potential disease relevance, we next thought to assess the expression of lncRNAs during cardiac disease by comparing the datasets obtained from sham-treated vs. TAC-treated mice. Upon increasing the clustering resolution from 0.3 to 0.7, a more detailed and granular cell assignment of lncRNA genes to cellular subtypes was achieved (Extended Data Fig. S2A

123 and S2B). With this setup, we performed differential gene expression analysis for the sub-populations
124 of the major cell types in the heart, and subset the resulting list to lncRNAs (Fig. 2A-C, Extended Data
125 Fig. S2C). Some lncRNAs were regulated after TAC throughout all subpopulations of a cell type, e.g.,
126 Gm29686 in fibroblasts (Fig. 2A), whereas others were only significantly regulated within a defined
127 subpopulation, e.g., Gm49785 in the fibroblast subpopulation (FB6) (Fig. 2A). This subpopulation of
128 fibroblasts represents activated myofibroblasts (high expression of periostin), a cell type involved in
129 extracellular matrix secretion and immune cell recruitment [28]. Similarly, several lncRNAs displayed
130 dysregulation within cardiac endothelial cells (Fig. 2B) and cardiac macrophages (Fig. 2C), resolved to
131 the level of cellular subtypes.

132 Of particular interest are lncRNAs in macrophages of the myocardium, since no lncRNA had thus far
133 been identified or functionally characterized in this cardiac cell type. As a first approach to the potential
134 function of the lncRNAs we had identified as deregulated in crMPs in the TAC model, we correlated
135 these lncRNAs with biological processes of their overlapping neighboring genes (Extended Data Fig.
136 S2D). Since lncRNAs are often co-expressed and co-regulated with proximal genes in *cis* [29], we
137 speculated that the latter may give insight into the biological context within which these lncRNAs
138 function. For example, genes antisense to downregulated lncRNAs in the Mac1 cluster (Lyve1+
139 macrophages) after TAC are associated with programmed cell death processes and genes antisense
140 to downregulated lncRNAs in the Mac2 cluster (Cd74+ macrophages) after TAC were predominantly
141 linked to adhesion pathways (Extended Data Fig. S2D), suggesting that the reported de-regulated
142 lncRNAs might also be involved in the regulation of these processes.

143 Taken together, we report a comprehensive inventory of regulated lncRNA genes in the major non-
144 myocyte cell types of the heart during pressure overload. These lncRNA genes will be interesting
145 candidates to be studied in more detail.

146 **Determination and annotation of the lncRNA landscape of cardiac resident macrophages**

147 As the sequencing depth of current single cell sequencing methodology limits detection sensitivity, we
148 therefore complemented our scRNA-seq data by performing deep RNA-Seq on basal total murine
149 myocardium as well as crMPs that were isolated using well-established cell markers (Cd45, Cd64,
150 Cd11b and F4/80 [9,10]). These surface proteins collectively labelled essentially all crMPs in our scRNA-
151 seq data (Extended Data Fig. S3A), corroborating our purification strategy. Using a pipeline to identify
152 and quantify novel lncRNAs (Extended Data Fig. S3B), we identified 250 genes that had previously not
153 been annotated by Gencode vM22 [18]. The identified novel lncRNAs showed the same characteristics
154 as the known lncRNAs with respect to having no coding probability (true non-coding) and transcript
155 length (Extended Data Fig. S3C upper panel), but were more highly expressed in our data set than the
156 known lncRNA population (Extended Data Fig. S3C lower panel). RNA-seq from fractionation
157 experiments showed for known lncRNAs a distribution of 80% in the nucleus (and 20% to the
158 cytoplasm), the novel lncRNAs are slightly less nuclear in localization (70% nuclear, 30% cytoplasmic
159 (Extended Data Fig. S3D).

160 As a further approach to the function of the newly identified lncRNAs, we built on the observation that
161 the products of lncRNA genes and protein-coding genes which are in proximity of 5kb or less and in
162 antisense overlapping orientation interact in the same biological processes [30]. The distribution of the

interaction categories (e.g. “antisense overlapping”) was comparable between novel and known lncRNAs (Extended Data Fig. S3E). Notably, 15 novel lncRNA genes were found without any interaction, categorizing them as novel long intergenic RNAs (lincRNA). For both known and novel lncRNAs we found many well-expressed genes (> 5 transcripts per million reads, TPM) that are specific in cardiac macrophages compared to total murine myocardium (containing myocytes, endothelial cells, fibroblasts, and macrophages) (Fig. 3A).

Identification of lncRNA *SchlafenInc* as an abundant and enriched macrophage lncRNA

In order to select lncRNA candidates for experimental validation, we further filtered the datasets from scRNA-Seq data and RNA-Seq based on the following stringent criteria: low coding probability according to CPAT score (true non-coding RNA < 44% coding probability), absolute expression > 25 TPM in macrophages, enrichment of $\log_2$FC >3 and FDR <0.05, and de-regulation in TAC (scRNA-seq data) FC >0.25). This yielded 13 lncRNA candidates that are highly abundant, enriched and regulated in cardiac macrophages (Fig. 3B).

We found one of these candidates, lncRNA *AI662270*, particularly interesting due to its genomic association with a cluster of eight genes on chromosome 11 which encode members of the Schlafen family of proteins (Fig. 3C). Schlafen proteins are found in human and mouse and known to regulate important processes and functions such as immune cell development, invasion and migration [31]. *AI662270*, however, is a hitherto uncharacterized gene within this locus. The genomic location of lncRNA *AI662270* in the Schlafen cluster led us to name the transcript *SchlafenInc.*

The Schlafen locus of protein-coding genes is very similar between human and mouse in general, yet the internal order of the proteins (and lncRNAs) is slightly different. A study by Ulitsky and colleagues developed a pipeline to identify syntenic genes across multiple organisms, where lncRNAs are tested on the relative location and orientation to orthologous protein-coding genes [32]. By comparing Gencode annotations [18] of human (V30) and mouse (vM21) with their pipeline, the gene *ENSG00000267074* was designated as the putative human *SchlafenInc* homolog (Fig. 3C). It is expressed in various human cell types of leukocyte origin (using the RNA-Get module Encode data sets [33], Extended Data Fig. S4A), making it an attractive molecule for studying the observed phenotypes in human cells. Besides the analysis of expression, we tested if the two lncRNAs share common potential binding partners using a pretrained deep neural network (DNN) [34] on eCLIP-seq data [35]. Indeed, the mouse *SchlafenInc* and human *ENSG00000267074* contain three major binding modules of the same or similar proteins (Extended Data Fig. S4B and S4C), supporting the hypothesis of conservation.

Murine *SchlafenInc* was up-regulated after TAC in both macrophage populations, but even more pronounced in Mac2 (MHCII-high, Cd74+) macrophages (Fig. 3D). Its strong expression made it readily detectable by Northern blotting (Fig. 3E). Interrogation of the RNA-seq datasets from the nucleus and the cytosol, as well as RNA *in situ* hybridization, showed that *SchlafenInc* localizes to both compartments (Fig. 3F and G, Extended Data Fig. S4D).

202 ***SchlafenInc* determines myocardial macrophage infiltration and polarization in response to**
203 **pressure overload**

204 To assess the phenotype of a macrophage-specific deficiency of *SchlafenInc in vivo*, we generated a
205 *SchlafenInc*$^{-/-}$ mouse line by CRISPR/Cas9 methodology and examined these mice under basal and
206 disease conditions. The entire gene body was targeted with specific sgRNAs, including the promoter
207 region upstream of *SchlafenInc* (determined by H3K4me3 signals in murine bone marrow-derived
208 macrophages, ENCODE data set ENCSR000CFF[36]) to abrogate all transcription from that locus
209 (Extended Data Fig. 5 A). Deletion was verified by PCR from genomic DNA (Extended Data Fig. 5 B).
210 The early compensation stage of the TAC model is characterized by sterile inflammation and both an
211 influx of monocytes as well as proliferation of resident macrophages. We therefore performed sham and
212 TAC surgery (Fig. 4 A) and analyzed the heart phenotype and monocyte/macrophage numbers after 6
213 days (Fig. 4 B). The heart weight of *SchlafenInc*-deficient mice was significantly reduced (Fig. 4 C) and
214 heart function (comparing ejection fraction of sham and TAC mice) was significantly improved (Fig. 4
215 D). Furthermore, *SchlafenInc*$^{-/-}$ hearts showed a substantial decrease in pressure overload-induced
216 interstitial fibrosis (Fig. 4 E) and interestingly a significantly reduced monocyte/macrophage infiltration
217 after TAC, as determined by immunostaining of left ventricular myocardial sections against the
218 monocyte/macrophage marker Cd68 (Fig. 4 F).

219 To assess the composition of immune cells in more detail we next performed scRNA-seq of the CD45+
220 cell fraction isolated from the myocardium and blood (Fig. 5 A). As expected, macrophages are the
221 dominant cell population within the heart whereas the blood contains more monocytes (Fig. 5 B).
222 Activated macrophages and monocytes release signals in an auto- and paracrine fashion[19]. *SchlafenInc*$^{-}$
223 $^{/-}$ mice showed decreased signaling between almost all macrophage and monocyte populations after 6
224 days of TAC (Fig. 5 C), with a significant decrease in inflammatory signaling pathways such as
225 Osteopontin (Spp1) and Macrophage Inhibitory Factor (Mif) signaling (Fig. 5 D). Both Osteopontin and
226 MIF are important factors in recruiting monocytes and other inflammatory cells from the blood after
227 cardiac injury[37,38]. Performing RNA velocity analysis of cardiac leukocytes after TAC (Fig. 5 E) showed
228 gene dynamics of *SchlafenInc* WT Ly6C-high monocytes towards non-classical monocytes as well as a
229 moderate dynamic from MHCII-high macrophages to Lyve1 macrophages. In *SchlafenInc*$^{-/-}$, the
230 dynamics between monocytes is abolished while transition dynamics from the monocyte-derived
231 macrophages (MHCII high) to resident macrophages (Lyve1) is strongly increased. This analysis
232 showed stronger polarization of cardiac macrophages towards the *Lyve1* macrophage population in the
233 *SchlafenInc*$^{-/-}$ heart which is generally believed to play a more anti-inflammatory role following cardiac
234 damage.

235 Next, we asked which genes were changing globally in Lyve1^{+} macrophages after TAC due to
236 *SchlafenInc* deletion. Among the genes that are de-regulated during TAC (WT TAC vs. sham), 64 genes
237 were additionally strongly de-regulated in *SchlafenInc*$^{-/-}$ vs. *SchlafenInc* WT Lyve1^{+} macrophages
238 (|Log2FC|>0.5, FDR<0.05). 17 of these genes are classified as coding for secreted proteins (Fig. 5 F,
239 categorization according to Human Protein Atlas[39]), for example, *Lgals3* (Galectin-3) and *Spp1*
240 (Osteopontin), which are de-regulated in all macrophage populations (Extended Data Fig. 5 C). An

241 analysis of the associated biological processes of de-regulated genes in Lyve1^{+} macrophages (Fig.5 F)
242 showed leukocyte chemotaxis and migration as the strongest impacted pathways (Fig. 5 G).

243 Taken together, *SchlafenInc* deletion in immune cells of the heart altered cardiac macrophage response
244 to early pressure overload towards an anti-inflammatory phenotype and disease-associated phenotypes
245 such as fibrosis and heart weight were improved.

246 ***SchlafenInc* is required for macrophage adhesion and migration**

247 To elucidate the function of *SchlafenInc* in more detail and explore its potential role in migration
248 processes, we generated *SchlafenInc*-deficient macrophages from Hoxb8-FL macrophage
249 progenitors[40,41] (Extended Data Fig. S6A). Gene deletion was validated by RNA-Seq (Extended Data
250 Fig. S6A, middle track). As a genomic deletion might have an impact on nearby genes due to a
251 mechanism in *cis* by the deleted lncRNA or due to the deletion of a regulatory element within the DNA,
252 the surrounding region of *SchlafenInc* (0.5 Mbp in each direction) was analyzed for de-regulation
253 (Extended Data Fig. S6B). 9 of 64 genes were found to be moderately dysregulated (with |log2FC| > 1,
254 FDR < 0.05) in the vicinity of *SchlafenInc* revealing that there was not a general activation or de-
255 activation of that locus by *SchlafenInc*. To identify major perturbations on gene expression level,
256 *SchlafenInc* KO monoclonal cell lines (2 clones, each measured in n=4) were subjected to RNA-Seq.
257 These samples were compared to control monoclonal cell lines (two clones with n=3 each) that were
258 generated using an unrelated sgRNA (sequenced as wildtype at the *SchlafenInc* locus). We observed
259 2,660 genes significantly de-regulated (|log2FC| > 1, FDR < 0.05) (Fig. 6 A), among those *SchlafenInc*
260 that dropped from 67 TPM to 0.33 TPM. Among the downregulated genes, we observed an enrichment
261 of genes involved in migration and adhesion similarly to our *in vivo* study (Fig. 6 B, e.g., *Mmp14* and
262 *Lgals3*). Lower amounts of *Lgals3* could not only be observed in our RNA-Seq data but were validated
263 on protein level (Galectin-3 is the gene product of *Lgals3*) by measurement of cell culture supernatant
264 using an enzyme-linked immunosorbent assay (ELISA) (Fig. 6 C). More generally, gene ontology
265 analysis of all significantly de-regulated genes implicated pathways such as regulation of cytokine
266 production, regulation of cell adhesion and chemotaxis that are promoted by *SchlafenInc* (Fig. 6 D). To
267 validate these results, we performed an adhesion assay by rigorous washing (Fig. 6 E) as well as tested
268 the chemotactic migration ability of *SchlafenInc* KO macrophages with a gradient of the chemokine C5a
269 (Fig. 6 F). Adhesion was diminished by approximately 23% (Fig. 6 E) and chemotaxis was about 50%
270 reduced (Fig. 6 F) in *SchlafenInc* KO cells compared to wild type controls.
271 Together these data obtained on *SchlafenInc*-deficient macrophages corroborate a cell autonomous
272 role for this lncRNA in macrophages, in line with its specific expression in this cell type. *SchlafenInc* is
273 required for the activation of macrophage gene programs underlying cell adherence and migration
274 providing a mechanistic basis for the phenotype observed in vivo for the *SchlafenInc*-deficient mice.
275
276
277
278
279

280 **DISCUSSION**

281 This study provides the first comprehensive lncRNome of cardiac resident macrophages. One of the
282 most highly enriched and abundant lncRNAs in cardiac resident macrophages – lncRNA *AI662270*,
283 which we termed *Schlafenlnc* – was shown to be involved in adhesion and migration. As for *Schlafenlnc*,
284 a particular characteristic of lncRNAs in general is their high degree of cell type-specificity[21–23] which
285 makes them important for processes such as development, differentiation of cell types, cellular fate and
286 function (reviewed in [3]). This characteristic could therefore make lncRNAs the natural choice when
287 describing cell population expression signatures, especially in single cell RNA sequencing (scRNA-seq).
288 scRNA-seq allows for an unbiased approach to identify main- and sub-populations of cells, yet little
289 focus has been set to expressly include lncRNA marker genes. Initially, methodical problems such as
290 library preparation, sequencing depth or analysis software hampered the detection of lncRNAs in such
291 data sets. LncRNAs are still not as readily measured as mRNAs due to their on average lower
292 expression levels, but together with improved scRNA-seq depth and improved annotations, our data
293 suggest that lncRNAs are underestimated markers of cell type definition. Emerging platforms measuring
294 RNA transcripts in tissue such as spatial transcriptomics or *in situ* sequencing (reviewed in [42]) might be
295 able to leverage that potential further.

296 Focusing on lncRNAs and their potential regulation in ventricular myocardium during disease, we
297 could identify an extensive set of regulated lncRNAs for all major cell populations. In general, we find
298 more up-regulated than down-regulated genes upon induction of disease, which we believe to be due
299 to the detection limit of scRNA-seq concerning very lowly expressed genes [43]. LncRNAs more specific
300 to and regulated in a subset of cell types might offer new possibilities for therapeutic intervention and to
301 gain insight into regulatory mechanisms specific for defined cell types. As we have shown for the three
302 macrophage clusters (Mac1 (Lyve1+), Mac2 (Cd74+) and transitional macrophages), the different sets
303 of regulated lncRNAs are implicated in distinct gene ontology pathways, which points to distinct
304 functions of these macrophage populations.

305 Cardiac resident macrophages have been shown to be key players in diseases such as heart failure
306 and myocardial infarction (reviewed in [44–47]). In the mouse model of left ventricular pressure overload,
307 crMPs are proliferating during the compensation phase (from 0 days to about 7-14 days). An infiltration
308 of monocyte-derived MPs starts early in disease and increases in the late, decompensated phase [48].
309 The infiltration of monocyte-derived MPs is typically associated with a long-term detrimental cardiac
310 function [48–55]. This recruitment of monocytes is at least to some degree dependent on crMPs[56], and
311 suppression of this communication axis might be beneficial. Galectin-3, for example, is known to be
312 increased in heart failure patients [57] and is associated with murine cardiac remodeling during pressure-
313 overload [58]. It is well known to be involved in the monocyte as well as macrophage migration and
314 infiltration in cardiovascular diseases [59–61]. Our combination of unbiased scRNA-seq measurements and
315 in-depth coverage by RNA-Seq allowed us to identify the hitherto uncharacterized lncRNA *Schlafenlnc*
316 as a regulator of macrophage adhesion and migration. *Schlafenlnc* is up-regulated after 6 days of TAC
317 as well as other genes involved in adhesion and migration such as Galectin-3 and its deletion impacts
318 Galectin-3 expression both *in vivo* and *in vitro*. Our quantitative assessment of macrophage/monocyte
319 numbers (Cd68 staining) and the analysis in relative immune cell composition by scRNA-seq after 6
320 days of TAC point to a mechanism of defective signaling by *Schlafenlnc* KO crMPs to initiate recruitment

321 of inflammatory cells such as monocytes. Given its selective expression in crMPs, we believe that
322 targeting of *Schlafenlnc* warrants further exploration as a potential anti-inflammatory therapeutic
323 strategy.
324 Similar to its orthologue in mice, human *Schlafenlnc* is specific for immune cell types (Extended Data
325 Fig. S4A). In support of conserved function in immune cells, our protein interactor analysis of both
326 murine and human *Schlafenlnc* using deep learning showed similar binding modules for RNA binding
327 proteins (Extended Data Fig. S4B and S4C). Further studies will be required to dissect molecular
328 interactors for *Schlafenlnc* in mouse and human.
329 Taken together, our study demonstrates that lncRNAs act as critical contributors to the
330 transcriptome-based analysis of cell clusters in line with their crucial role in development and cell fate
331 determination [3], leading to the definition of cell identities. The combination of single cell sequencing and
332 RNA-Seq approaches led us to the identification of multiple novel candidate lncRNAs that warrant
333 further analysis in cardiac homeostasis and disease. One of the most abundant and macrophage-
334 enriched lncRNAs, *Schlafenlnc*, acts as a crucial regulator of macrophage adhesion and migration.
335
336
337 **METHODS**

338 Experimental animals, surgery conditions

339 Surgeries on mice were performed according to the guidelines and regulations of the responsible
340 authorities. Consent was given by the institutional review board of the Regierung of Oberbayern (ROB-
341 55.2-2532.Vet_02-19-194).
342 Wild type male mice of C57BL/6N background were purchased from Jackson Laboratories and
343 submitted to transverse aortic constriction (TAC) or sham procedure as reported previously [16] at an age
344 of 8-10 weeks.

345 To produce *Schlafenlnc* -knockout mice, two sgRNAs (5' cut site: 5'- GAGGTTCCATCAGTCTGACA-
346 3', 3' cut site: 5'-ACATGTCTTTGGTAGGAGCA-3') targeting the flanking region of the *Schlafenlnc* gene
347 in the mouse genome were designed and synthesized by IDT (Coralville, IA, USA). A mixture of Cas9
348 protein (IDT) and sgRNAs was electroporated into C57BL/6 mouse zygotes. Genomic DNA of newborn
349 mice was amplified using the primers Slfnlnc1 (5'-TTCCTTCAGAGGTCCATCAG-3') and Slfnlnc4 (5'-
350 AGCCAGTCTAAAGACTCTGG-3'). The appearance of a 360 bp band identified founder mice with a
351 complete loss of the *Schlafenlnc* gene. The animals were bred to homozygosity and used for the
352 experiments.

353 Echocardiography was performed as reported before[16].

354 Primary cell isolation from adult murine heart

355 Hearts of C57BL/6N mice were harvested at an age of 8-10 weeks and subjected to digestion by
356 perfusion via the coronary arteries using Collagenase II (Worthington, Lakewood, NJ) as described
357 previously [62]. Cell suspension was processed according to subsequent protocol/experiment.

358 Single cell cloning and sequencing

359 Primary cells from a sham [16] and an adult mouse heart 6d after TAC were washed three times with PBS
360 to remove cell debris and passed successively through 100µm, 70µm and 30µm filters. The single cell
361 library was generated using the Chromium Single Cell 3' GEM, Library & Gel Bead Kit v2 (10X
362 Genomics) with a target of 10,000 cells per sample. The single cell library was cloned according to the
363 manufacturer's instructions. Sequencing was performed on a HiSeq4000 (Illumina).

364 Primary cells from the hearts from *SchlafenInc*-knockout and littermate wildtype mice in basal condition
365 as well as after 6d TAC were passed through a 100µm filter and centrifuged for 1min at 100*xg* to pellet
366 cardiomyocytes. The supernatant (non-myocytes) was passed through a 40µm filter and washed twice
367 in magnetic-activated cell sorting (MACS) buffer (PBS + 0.5% BSA + 2mM EDTA) to result in 200µl cell
368 suspension. For the isolation of PBMCs, blood was diluted with 5 ml of MACS buffer and layered onto
369 5ml of Ficoll-Paque (17144002, Cytiva), followed by centrifugation at 400xg and 4°C for 30min in a
370 swinging rotor without a brake. The white layer containing the cells was aspirated, transferred to a 50ml
371 tube and mixed with 30ml of MACS buffer. After centrifugation for 5 min at 300xg and 4°C, the pellet
372 was washed once more with 30ml MACS buffer (200xg and 4°C for 5min) and resuspended in 200µl
373 MACS buffer. Cardiac and blood leukocytes (basal condition) were further purified using MACS, labelled
374 with cell hashing antibodies and isolated by FACS (all steps at 4°C): Cell suspensions were incubated
375 with Fc-block (1:50, BD Pharmingen 553142) for 10min and subsequently incubated with mouse Cd45
376 MicroBeads (Miltenyi Biotec) for 15min. Cells were washed with MACS buffer and MACS was performed
377 using an AutoMACS (Miltenyi Biotec) running the program *possel_s*. After elution, pelleted cells were
378 resuspended in MACS buffer containing anti-Cd45-FITC (1:1000, clone 30-F11, Biolegend 103108), PI
379 (1:100) and cell hashing antibodies (1:1000, #1 for heart, #2 for blood, Biolegend) and incubated for
380 30min protected from light. For TAC samples, PBMCs were purified as above, cardiac non-myocytes
381 were directly used for cell sorting. Both cell fractions were stained with cell hashing antibodies (1:1000,
382 #2 for heart, #3 for blood, Biolegend) and PI (1:100) and incubated for 30min. After washing, live cells
383 of all samples were sorted on a Sony cell sorter SH800S, heart and blood cells of each genotype and
384 condition were pooled and run on a Chromium controller using the Chromium Next GEM Single Cell 3'
385 v3.1 Library & Gel Bead Kit (10X Genomics) with a target of 10,000 cells per pool. Libraries were cloned
386 according to the 10x Genomics user guide with feature barcode technology for cell surface protein
387 (RevD) and Biolegend's protocol for amplification of the cell hashing libraries. Libraries were pooled
388 according to the recommendations of 10x genomics protocol and sequenced on a NovaSeq6000
389 (Illumina).

390 Purification of primary cells and cardiac macrophages by F4/80 MACS and cell sorting for RNA-seq

391 For a total myocardial cell sample, 100µl of the raw cell suspension of primary cells from adult wildtype
392 mouse hearts were washed twice with PBS and lysed in Trizol (ThermoFisher) for subsequent RNA
393 preparation. For the purification of cardiac macrophages, the cell suspension was filtered through cell
394 sieves of 70µm and 40µm of size and centrifuged at 100 *x g* for 3min at 4°C to completely remove
395 cardiac myocytes. All following steps were performed on ice/at 4°C. The supernatant (non-myocytes)
396 was washed twice in magnetic-activated cell sorting (MACS) buffer (PBS + 0.5% biotin-free BSA + 2mM

397 EDTA). MACS was performed in a two-step process using anti-F4/80-biotin coupled antibody and
398 Streptavidin microbeads (Miltenyi Biotec) on LS columns. The eluted macrophage fraction was
399 resuspended in a final volume of 200µl MACS buffer and incubated 10 min with Fc block (1:50). 200µl
400 of staining solution containing flow cytometry antibodies (anti-Cd45-PECy7, anti-Cd64-PEDazzle594,
401 anti-Cd11b-PE) was added and incubated for 30min in the dark. Cells were washed twice with MACS
402 buffer and sorted on a Biorad S3 cell sorter. Cd45+/Cd64+/Cd11+ macrophages were collected
403 (between 100k-170K cells), washed with PBS and lysed in Trizol (Invitrogen) for RNA preparation.

404 Fibrosis staining

405 Paraffin sections (8 µm) of ventricular myocardium were stained with Sirius red and Fast green. Images
406 of the whole heart were taken with a 10x objective using a AxioObserver.Z1 (Zeiss, Jena, Germany)
407 motorized scanning-stage microscopy (130 x 85; Märzhäuser, Wetzlar, Germany). Fibrosis of the left
408 ventricular myocardium was quantified as the ratio of signals from Sirius red to Fast green in each
409 section using the Metamorph software (Molecular Devices).

410 Cd68 staining

411 Cryosections (5 µm) of ventricular myocardium were fixed with methanol for 10 min at -20°C, washed
412 thoroughly with tap water and treated with acetone for 1 min at -20°C. Sections were air dried and
413 subsequently blocked with 5% goat serum in PBS for 1 h. Sections were stained with anti-mouse Cd68
414 (1:100) (AbD Serotec, MCA 1957) at 4°C overnight. The sections were washed three times with PBS +
415 0.05 % Tween 20 and stained with anti-rat AF564 (1:100) and Cytox Green (1:1000). Images were
416 acquired by confocal microscopy using 63x glycerol objective (Leica SP5) and analyzed using
417 Metamorph (Molecular Devices).

418 Generation of knockout macrophages

419 Conditionally immortalized hematopoietic progenitor cells were generated from a R26-Cas9-eGFP
420 transgenic mouse line [41] as previously described [40]. For inducing CRISPR-Cas9 mediated knockout in
421 Hoxb8-FL cells, cells were electroporated with an sgRNA pair targeting the *Schlafenlnc* locus (IDT: Alt-
422 R® CRISPR-Cas9 sgRNA, 5' cut site 5'-GAGGTTCCATCAGTCTGACA-3', 3' cut site 5'-
423 GGCTTGGAAGTAGAAAACCG-3'), as control, a single sgRNA was used (5'-
424 ACCCCTTCAGCTTCACCTCC-3'). Transfected cells were single-cell cloned by limiting dilution assay
425 into 96-well plates and screened for knockout clones. CRISPR-directed deletions on *Schlafenlnc* were
426 identified by a PCR-based strategy to amplify the genomic DNA of the clones. Single-cell clones carrying
427 the induced deletions were expanded and frozen for further use. To do this, extraction of genomic DNA
428 was performed with QuickExtract™ DNA Extraction Solution (Lucigen) according to the manufacturer's
429 instruction. Briefly, approximately 100,000 cells were lysed in 50µl of QuickExtract by incubation as
430 follows: 65°C – 15min, 68°C – 15min, 98°C – 10min. 50ng of genomic DNA was then subjected to PCR
431 amplification with two primer pairs to distinguish successful *Schlafenlnc* knockout clones from wildtype
432 or heterozygous knockout. *Schlafenlnc*_KO_forward 5'-CAGCCCTGAGTCAGAACATAC-3' and
433 *Schlafenlnc*_KO_reverse 5'-TCCTTAGGGTGCACATCTACT-3' were used for detection of a
434 successfully cut site with a resulting amplicon length of 480bp, *Schlafenlnc*_WT_forward 5'-

435 TCTGTCTCTACTCCCTCAACTC-3‘ and *Schlafenlnc*_WT_reverse 5‘-AAGGCATGTTCTGCTCCTAC-
436 3‘ were used for detection of the wildtype allele/uncut gene locus with a resulting amplicon length of
437 320bp.

438 Hoxb8-FL *Schlafenlnc* KO cell culture and differentiation

439 Hoxb8 progenitor cells were cultured in RPMI 1640 supplemented with 10% FCS, 1% Pen/Strep, 50
440 ng/mL FLT3L, 50nM b-mercaptoethanol and 1nM b-estradiol. FLT3L supernatant was obtained from a
441 FLT3L-producing B16 melanoma cell line.
442 For differentiation of HoxB8 cells into macrophages, Hoxb8 progenitor cells were cultured in
443 differentiation medium consisting of the culturing medium described above without b-estradiol and
444 supplemented with 20% MCSF supernatant, which was obtained from a MCSF-producing L929 cell line.
445 Differentiation was accomplished after 6 days.

446 Generation of bone marrow-derived macrophages

447 Femurs and tibias from 6-12 week old C57BL/6N mice were prepared and bone marrow was isolated
448 by flushing the bones with R10 medium (RPMI medium, 10% FCS, 1% antibiotics) with a syringe. To
449 generate bone marrow derived macrophages, 3-4 mio. isolated bone marrow cells were seeded in a
450 10cm petri dish containing R10 medium supplemented with 20% MCSF supernatant. Medium was
451 added on day 3 and exchanged on day 6 after seeding, macrophages were fully differentiated on day 8
452 and used for experiments.

453 Cytoplasmic/nuclear fractionation

454 Cytoplasmic/nuclear fractionation was performed as described before [63]. Briefly, bone marrow-derived
455 macrophages (BMDMs) were washed two times with cold PBS and harvested. 10% of the cells was
456 transferred into a new tube and used as a sample for the total gene expression. Cells were centrifuged
457 at 200 *x g* for 10 minutes and the total expression sample was directly used for RNA isolation. The
458 fractionation sample was resuspended in 200µl lysis buffer A (10 mM Tris pH=8, 140 mM NaCl, 1.5 mM
459 MgCl2, 0.5% Nonidet P-40) and incubated for 5 minutes on ice. The lysate was centrifuged at 1000 *x g*
460 for 3 minutes at 4°C. The supernatant containing the cytoplasmic fraction was directly used for RNA
461 isolation through lysis with Trizol. The sediment containing the nuclear fraction was washed two times
462 with lysis buffer A and one time with lysis buffer B (Buffer A supplemented with 1% Tween-40, 0.5%
463 deoxycholic acid) and afterwards resuspended in Trizol for RNA isolation.

464 RNA cloning and sequencing

465 Libraries from primary cardiac macrophages and total myocardium as well as *Schlafenlnc* KO and
466 control cell lines were generated using the TruSeq Stranded RNA Kit (Illumina) according to the
467 manufacturer’s protocol, except for one step. Instead of using the SuperScriptII (ThermoFisher) as the
468 reverse transcriptase, SuperScriptIII (ThermoFisher) was used at a reaction temperature of 50°C.
469 Sequencing was performed on a HiSeq4000 platform (Illumina).

470 Libraries from fractionation samples were generated using the Stranded mRNA Prep, Ligation Kit
471 (Illumina) according to the manufacturer's instructions. Sequencing was performed on a NovaSeq6000
472 machine (Illumina).

473 RNA *in situ* hybridization (RNAscope)

474 Bone marrow derived macrophages were seeded on a removable 8-well chambers slide (Ibidi) and RNA
475 *in situ* hybridization was performed using the RNAscope Fluorescent Multiplex Reagent Kit (Advanced
476 Cell Diagnostics (ACD)) according to manufacturer's instructions. A custom designed RNA probe by
477 ACD was used for detection of *Schlafenlnc* (ENSMUST00000143673.2). Following the RNA *in situ*
478 hybridization, the slides were incubated with Phalloidin-AF647 (Abcam) for 60 minutes at room
479 temperature. Subsequently, slides were washed three times with PBS and mounted using ProLong™
480 Gold Antifade Mountant (Invitrogen). Images were acquired using the confocal microscope Leica TCS
481 SP II and the Leica Application Suite.

482 Galectin-3 ELISA

483 Cell culture supernatant of differentiated Hoxb8 macrophages was collected and the amount of soluble
484 Galectin-3 was quantitatively assessed using the Galectin-3 Mouse SimpleStep enzyme-linked immuno-
485 sorbent assay (ELISA) kit (Abcam) according to the manufacturer's instructions. The cell culture
486 supernatant was diluted 1:10 in sample diluent before use.

487 Chemotaxis

488 An IncuCyte® ClearView 96-Well Chemotaxis Plate (Sartorius) was coated on both sides of the
489 membrane using 50 µg/mL Matrigel (Corning) at 37°C for 30 minutes. After coating, plates were
490 incubated at room temperature for 30 minutes and afterwards washed with D-PBS. Differentiated HoxB8
491 macrophages were harvested and 2,000 cells were seeded in each well in differentiation medium
492 containing 0.5% FCS. Cells were allowed to settle at the bottom of the upper well for 30 minutes.
493 Subsequently, 100nM recombinant murine C5a (Pepro Tech) was added to the lower well of the
494 ClearView migration plate. Cells were imaged every 2 h for 72 hours using an Incucyte ZOOM
495 instrument and a 10x objective with chemotaxis plate settings. Chemotaxis was analyzed using the
496 IncuCyte ZOOM software.

497 Adhesion Assay

498 Ibidi black 96 well µ-Plate was coated with 20µg/mL Fibronectin (Sigma Aldrich) for 1 h at 37°C. 10,000
499 differentiated Hoxb8 macrophages were seeded in each well in differentiation medium and were
500 incubated for 2 hours at 37°C in a 5% CO2 atmosphere. After the incubation, cells were stained using
501 NucBlue Live ReadyProbes reagent (Invitrogen) and following the manufacturers' instructions. Images
502 of the Nuclei were taken before and after removing the non-adherent cells by washing three times with
503 pre-warmed medium using an EVOS FL Auto 2 cell imaging system (Invitrogen). Cell nuclei were
504 counted automatically using the MetaMorph analysis software (Molecular Devices).

505

506 Northern blotting

507 Northern blotting was performed as reported previously [64]. Briefly, 10µg total RNA from fibroblasts
508 (NIH/3T3) and in vitro differentiated macrophages were run on a 1.2% formaldehyde agarose gel,
509 transferred to a Hybond-N+ membrane (Ge Healthcare) and UV-crosslinked. Probes were end-labelled
510 using [gamma-^{32}P]-ATP and purified using an Illustra ProbeQuant G-50 micro column (GE Healthcare).
511 A mixture of two different probes was used per target. Probes were incubated over night with a pre-
512 hybridized membrane, signal was accumulated using a phophoimager screen and detected using a
513 Cyclone Plus (PerkinElmer). mGAPDH probe1 5'-
514 CATGGACTGTGGTCATGAGCCCTTCCACAATGCCAAAGTTG-3', mGAPDH probe2 5'-
515 GAATTTGCCGTGAGTGGAGTCATACTGGAACATGTAGACCATGTAGTTGAGG-3', Slfnlnc probe1
516 5'-CAGCTCTGCGTCTCTGCTCCTGTTCAGGTCCATCTTTCATCTCCG-3', Slfnlnc probe2 5'-
517 CAGTCGGGGTTCTGCCTCTTGATGTGGTTGTGCTAACCGGTGGGAC-3'.

518 Quantitative real-time PCR

519 1 µg of total RNA was reverse transcribed with Protoscript II reverse transcriptase (NEB), both according
520 to the manufacturer's instructions using random hexamer primers. Quantitative real-time PCR (qPCR)
521 was carried out with primers listed below, using the FastStart universal SYBR Green master mix
522 (Roche). The sample volume of 12.5 µl contained 1x SYBR Green master mix, 5 pmol of each primer
523 and 10 ng of cDNA. PCR was performed using StepOnePlus Real-Time PCR systems (Applied
524 Biosystems). Slfnlnc_qPCR fwd 5'- ATGACTGGTCCTGGTTTTCG -3', Slfnlnc_qPCR fwd 5'-
525 TCTGCCTCTTGATGTGGTTG -3', mRPL32 fwd (housekeeping gene) 5'-
526 ACATCGGTTATGGGAGCAAC -3', mRPL32 rev (housekeeping gene) 5'-
527 GGGATTGGTGACTCTGATGG -3'.

528 Data analysis

529 *Single cell sequencing data analysis*
530 Raw reads generated by single cell RNA sequencing data from sham[16] and 6d after TAC (this study)
531 was aligned against the mouse genome (mm10, Gencode annotation vM22 [18]) using CellRanger 5.0.0
532 (10x Genomics). Cell that were called by CellRanger were subsequently analyzed using the R package
533 Seurat v3.2 [65]. After quality control (retaining cells with >500 or <3,600 detected genes, <10%
534 mitochondrial cell content), 7,913 cells of the sham condition and 13,803 of the TAC condition were
535 used for further downstream analysis. SCTransform [66] was used to normalize and scale the data as well
536 as remove unwanted variation (regressing out mitochondrial gene content and cell cycle score).
537 SCTransform was then applied to identify variable feature which were used to integrate both data sets
538 ("IntegrateData" function). By using the ElbowPlot function on Principal Component Analysis results, the
539 number of relevant components was determined (set to 40) and used for embedding and visualization
540 by Uniform Manifold Approximation and Projection (UMAP). Seurat's "FindAllMarkers" function was
541 used for determination of cell population marker genes.
542 For the comparison of clusterings with adjusted Rand index score, gene sets were defined as follows:
543 all genes = all genes listed in the vM22 annotation of Gencode; protein coding genes = all genes with

544 gene biotype “protein coding” in vM22; lncRNAs = all genes in vM22 lncRNA annotation of Gencode
545 (gene biotype “lncRNA”+“TEC”); “expressed” gene sets = same definitions as above with filter for
546 average expression >0 in at least one cell cluster; all variable genes = gene list generated by Seurat’s
547 “SelectIntegrationFeatures”, default is 3,000 genes; subset of variable genes based on gene lists
548 defined above. Next, clusterings with resolutions from 0.01 to 1.00 with 0.01 increments were iteratively
549 calculated (“FindClusters” function) and cluster ID per cell was saved in a data frame. The adjusted
550 Rand Index is a measure for the degree of similarity between two clusterings, for example. The R
551 package mclust [67] with inbuilt function “adjustedRandIndex” was used to compare all gene sets to the
552 respective complete gene set (e.g. the subset of expressed lncRNAs to all expressed genes).
553 For calculating de-regulated genes after TAC, first Adaptively thresholded Low-Rank Approximation
554 (ALRA) [68] was performed in order to impute drop out gene expression values followed by using Seurat’s
555 “FindMarkers” function to compare each cell population before and after TAC.
556 For the analysis of scRNA-seq data of *Schlafenlnc* KO and WT animals, raw reads from basal and 6d
557 after TAC from WT and KO were aligned against the mouse genome (mm10, Gencode annotation
558 vM25[18]) using CellRanger 6.0.1 (10x Genomics) and analyzed using the R package Seurat v3.2 [65].
559 Quality control was applied to basal (>200 or <5,000 detected genes, <10% mitochondrial cell content)
560 and TAC (>200 or <4,000 detected genes, <10% mitochondrial cell content) samples. SCTransform and
561 FindAllMarkers was applied as above to normalize, scale, integrate data and identify marker genes for
562 cell populations. The integrated object was subset on all cell clusters expressing Cd45 (Leukocytes).
563 Deregulated genes were calculated using Seurat’s “FindMarkers” function to compare each cell
564 population between *Schlafenlnc* KO and WT. GO Term analysis of the deregulated genes was
565 performed using “DAVID 2021” [69].

566 *Cell-cell communication analysis*

567 A subset of cells of interest from blood and heart of *Schlafenlnc* KO and WT CD45+ (*Lyve1*
568 macrophages, *MHCII*-high macrophages, *Isg* macrophages, intermediate macrophages, classical
569 monocytes and non-classical monocytes) was used for analysis of secreted signaling pathways within
570 the CellChat database. The *Schlafenlnc* KO and WT objects were analyzed separately using CellChat[70]
571 and merged with “mergeCellChat”. The differential number of interactions between the cell clusters in
572 *Schlafenlnc* KO vs. WT was analyzed and displayed using the CellChat function
573 “netVisual_diffInteraction” and the differential signaling pathways were assessed using “rankNet”.

574 *Estimating RNA velocity*

575 To calculate the RNA velocity of single cells, the abundance of the spliced and unspliced RNA was
576 quantified by running Velocyto CLI (v0.17.5) on CellRanger output BAM files and the corresponding
577 gene annotation (GENCODE vM22). The resulting loom files were incorporated into the Seurat objects
578 using SeuratWrapper R package (v0.3.0), and after integration and clustering, the objects were
579 converted to AnnData format (h5ad) to be compatible for downstream analysis with the Python package
580 scVelo (v0.2.5). Using scVelo, cell-to-cell transition probabilities were estimated and RNA-velocity was
581 projected as streamlines on the UMAP embedding.

582

583 *Identification of novel lncRNAs*

584 Most steps of this pipeline were performed using the Galaxy platform [71]. Reads were mapped using
585 RNA STAR aligner (Galaxy version 2.6.0b-2) [72] using a built-in index based on Gencode vM22
586 annotation and otherwise default parameters. StringTie (Galaxy Version 1.3.3.2) [73] was used to predict
587 novel transcripts (strand information RF, reference file Gencode vM22, average read length 90).
588 StringTie merge (Galaxy version 1.3.6) with default parameters was used to merge all new annotations
589 together, including Gencode annotation vM22 as reference annotation. Novel genes were extracted by
590 Bedtools Intersect tool (Galaxy version v2.29.0) [74], intersecting the merged annotation with the Gencode
591 vM22 annotation. Transcripts were extracted with the "Extract features" tool (Galaxy 1.0.0) and analyzed
592 for coding potential with FEELnc (Galaxy version 0.1.1.1) [30]. FEELnc produces a gene transfer format
593 (gtf) annotation file containing only transcripts classified as long non-coding RNAs. "cat" command was
594 used to merge this lncRNA annotation to Gencode vM22 reference annotation file to create reference
595 annotation file with additional novel lncRNA genes. All RNA-Seq libraries were measured again against
596 this new transcriptome using StringTie's "count" option. For visualizing coding probability, the python
597 version of the Coding-Potential Assessment Tool (CPAT, v2.0.0) [75] was run on the fasta sequences of
598 the novel lncRNAs ($ cpat.py -g novel_lncRNAs_gffread.fasta -d Mouse_logitModel_CPAT.RData -x
599 Mouse_Hexamer_CPAT.tsv -o output_novel_lncRNAs.txt). GraphPad Prism 8 was used to calculate
600 the frequency distribution in percentages. For plotting transcript lengths, the length determined in the
601 CPAT output was used and again transformed to frequency distribution in Prism. For the categorization
602 of interactions between lncRNAs and other genes, the classifier output of FEELnc was used.
603 Interactions with the same gene were discarded, for known lncRNAs only genes expressed
604 predominantly in cardiac macrophages were considered ($\log_2$ fold change >1). To compute differential
605 gene expression analysis, DESeq2 package was used (Galaxy version 2.11.40.2) [76], outputting also a
606 normalized counts file. Normalized counts served as input for clustering and heatmap visualization by
607 ClustVis R package (v. 0.0.0.9) [77].

608 *RNA-Seq analysis of Hoxb8 Schlafenlnc KO macrophages*

609 Fastq reads were mapped using RNA STAR aligner (Galaxy version 2.6.0b-2) [72] using a built-in index
610 based on Gencode vM22 annotation and otherwise default parameters. StringTie (Galaxy Version
611 1.3.3.2) [73] count option was used to quantify gene expression using Gencode vM22 as reference
612 annotation. DESeq2 was used to calculate differential gene expression (Galaxy version 2.11.40.2) [76].
613 The normalized counts file was used for heatmap visualization with ln(x) transformation of the top 20
614 down-regulated genes (ClustVis R package [77]).

615 *Neighboring genes analysis and Gene Ontology Analysis*

616 Up- or downregulated lncRNAs during pressure overload (p-value<0.05) in either macrophage,
617 fibroblast or endothelial cell populations were analyzed for neighboring genes using FEELnc (Galaxy
618 Version 0.2, [30]) and filtered for antisense protein coding genes. Gene ontology analysis for these gene
619 sets for each cell population was performed using the web-based tool "DAVID 2021" [69]. Neighboring
620 genes of known and novel lncRNAs were also identified using FEELnc (Galaxy Version 0.2, [30]).

621 Biological processes associated with the differentially regulated genes in *Schlafenlnc* KO
622 macrophages (log2FC > 1 or < -1, FDR < 0.05) were determined using ClueGO application (v2.5.8) [78]

623 ran within Cytoscape (v3.8.2) [79] network analysis tool (p-value cutoff = 0.01, Min GO level = 4, Max GO
624 Level = 10, Number of Genes = 2, Min. Percentage = 4.0).

625 *Kipoi RBP-eclip analysis (Protein interactors analysis)*
626 Model training data: To access the binding probability of known RBPs on *Schlafenlnc*, a pretrained deep
627 neural network (DNN) [34] on eCLIP-seq data [35] was downloaded from the Kipoi repository [80]. In order to
628 test the binding probability of the 101 proteins on *Schlafenlnc*, a bed file containing the coordinates of
629 *Schlafenlnc*'s 4 exons (ENSMUST00000143673.2 on Ensembl) was obtained. Then for each exon, we
630 took sliding windows of 101nt length resulting on a new bed6 file where each row is of 101nt length.
631 Kipoi builds on environments, making the sharing and loading of models easy. We started our analysis
632 by generating an environment with all the needed dependencies. Afterwards for each protein of interest,
633 we programmatically obtained the dataloader, load the fasta sequence for GRCm38.p6, load the
634 GENCODE annotation for mouse version vM22 [18], and a bed file with the pre-extracted 101nt length
635 sliding windows and ran the predict function with default arguments (considering all the genomic
636 landmarks also for non-protein coding genes). Finally, for each protein of interest a csv file was
637 generated, containing the following info for each 101nt sequence considered: the chromosome, the
638 starting position, the end position, a sequence ID, a score as in the bed6 file, the strand and the binding
639 score [0 (no binding probability), 1 (high binding probability)] of the protein of interest on that window.

640

641 <u>Software list</u>

642 Leica Application Suite Advanced Fluorescence, version 2.7.9723
643 Invitrogen EVOS FL Auto 2 Software
644 CellRanger, version 5.0.0
645 Seurat, version 3.2
646 RNA STAR aligner, version 2.6.0b-2
647 StringTie amd StringTie merge, version 1.3.3.2 and 1.3.6
648 Bedtools Intersect tool, version v2.29.0
649 "Extract features" tool, version 1.0.0
650 FEELnc, version 0.1.1.1 (Galaxy) and version 0.2
651 Coding-Potential Assessment Tool, CPAT, version 2.0.0
652 DESeq2, version 2.11.40.2
653 ClustVis R package, version 0.0.0.9
654 Cytoscape, version 3.8.2
655 ClueGO, version 2.5.8
656 MetaMorph Offline, version 7.10.1
657 Prism 8 for Mac OS, version 8.4.1
658 Adobe Illustrator for Mac OS, version 24.2.1
659 R studio, version 3.6.3
660 Microsoft Office for Mac

661 Statistical Analysis

662 All data on bar graphs are presented as mean ± standard error of the mean (SEM). The
663 nuclear/cytoplasmic distribution of lncRNAs of the BMDM fractionation experiments is reported as violin
664 plots with median and quartiles. The chemotaxis assay is represented as xy-plot with mean ± standard
665 error of the mean (SEM). The ARI calculations are displayed as boxplot with median and quartiles.
666 Statistical analysis was performed using GraphPad Prism 8. Data distribution and the difference
667 between variances were tested using the Kolmogorov–Smirnov. Depending on the distribution of data,
668 unpaired t-test or Mann–Whitney test were used to determine statistical significance. For chemotaxis
669 experiments, statistical significance was tested using repeated measures two-way ANOVA followed by
670 Sidak correction. Significance is depicted as $*p < 0.05$, $**p < 0.01$, $***p < 0.001$, $****p < 0.0001$. The
671 detailed statistical analyses are provided as a Source Data file.

672

673 **ACCESSION NUMBERS**

674 All sequencing data sets can be accessed at GEO database under GSE210732.

675

676 **ACKNOWLEDGEMENT**

677 We thank Lucia Koblitz for expert support with primary cell preparations, Julia Kerler and Anton Bomhard
678 for expert assistance in animal surgeries and Dr. Elisabeth Graf for assistance with RNA-seq. We thank
679 Dr. Daniel Andergassen and Dr. Bernhard Laggerbauer for critical reading and helpful discussions.

680

681 **FUNDING**

682 This project was funded by the Deutsche Forschungsgemeinschaft (DFG, German Research
683 Foundation)—Project- ID 403584255–TRR 267 (S.E., A.D., R.P.B., M.S.L., L.M., T.M., J.G.). S.E., A.D.,
684 L.A., D.E., K.H., N.P., H.S., C.S., T.W., J.G., E.T., H.B.S., T.M., N.J., M.S.L. and R.P.B. were supported
685 in the framework of the German Centre for Cardiovascular Research (DZHK), and the partner site in
686 Munich (MHA) (S.E., A.D., H.S., C.S., T.W., J.G., H.B.S., T.M.) projects 81X3600404 (A.D.),
687 81X2600245 (C.S.) and 81X2600246 (C.S.) or partner site RheinMain, Frankfurt (N.J., M.S.L. and
688 R.P.B.). S.E. and D.R. were supported by DFG through the Research Training Group GRK2338 and
689 the European Union's Horizon 2020 research and innovation programme under the Marie Skłodowska-
690 Curie grant agreement no. 813716.

691

692 **Author contributions**

693 A.D. and S.E. designed the study and wrote the manuscript. A.D., L.A. D.E., S.B., E.T., K.H., N.P. and
694 A.U. performed the experiments or analyzed the resulting data. M.B. provided the *Schlafenlnc* knockout

mouse. R.P.B., J.G., P.K., M.S.L., L.M., T.M., D.R., H.B.S., M.S.-S., C.S. and T.W. provided experimental models, instruments and crucial expertise. All authors read, commented on and approved the manuscript.

CONFLICT OF INTEREST

None declared.

REFERENCES

1. Goodall, G. J. & Wickramasinghe, V. O. RNA in cancer. *Nat. Rev. Cancer* **21**, 22–36 (2021).
2. Aliperti, V., Skonieczna, J. & Cerase, A. Long non-coding rna (Lncrna) roles in cell biology, neurodevelopment and neurological disorders. *Non-coding RNA* **7**, (2021).
3. Anderson, K. M. & Anderson, D. M. LncRNAs at the heart of development and disease. *Mamm. Genome* **33**, 354–365 (2022).
4. Wysoczynski, M., Kim, J., Iv, J. B. M. & Uchida, S. Macrophage Long Non-Coding RNAs in Pathogenesis of Cardiovascular Disease. (2020).
5. Klattenhoff, C. A. *et al.* Braveheart, a long noncoding RNA required for cardiovascular lineage commitment. *Cell* **152**, 570–583 (2013).
6. Li, K. *et al.* A noncoding antisense RNA in tie-1 locus regulates tie-1 function in vivo. *Blood* **115**, 133–139 (2010).
7. Micheletti, R. *et al.* The long noncoding RNA Wisper controls cardiac fibrosis and remodeling. *Sci. Transl. Med.* **9**, (2017).
8. Zaman, R. & Epelman, S. Resident cardiac macrophages: Heterogeneity and function in health and disease. *Immunity* **55**, 1549–1563 (2022).
9. Gomez Perdiguero, E. *et al.* Tissue-resident macrophages originate from yolk-sac-derived erythro-myeloid progenitors. *Nature* **518**, 547–551 (2015).
10. Epelman, S. *et al.* Embryonic and adult-derived resident cardiac macrophages are maintained through distinct mechanisms at steady state and during inflammation. *Immunity* **40**, 91–104 (2014).
11. Dick, S. A. *et al.* Three tissue resident macrophage subsets coexist across organs with conserved origins and life cycles. *Sci. Immunol.* **7**, 1–19 (2022).
12. Hulsmans, M. *et al.* Macrophages Facilitate Electrical Conduction in the Heart. *Cell* **169**, 510-522.e20 (2017).
13. Grune, J. *et al.* Neutrophils incite and macrophages avert electrical storm after myocardial infarction. *Nat. Cardiovasc. Res.* **1**, 649–664 (2022).
14. Fujiu, K. *et al.* A heart-brain-kidney network controls adaptation to cardiac stress through tissue macrophage activation. *Nat. Med.* **23**, 611–622 (2017).
15. Cahill, T. J. *et al.* Tissue-resident macrophages regulate lymphatic vessel growth and patterning in the developing heart. *Dev.* **148**, (2021).

733 16. Ramanujam, D. *et al.* MicroRNA-21–Dependent Macrophage-to-Fibroblast Signaling
734 Determines the Cardiac Response to Pressure Overload. *Circulation* **143**, 1513–1525 (2021).
735 17. Butler, A., Hoffman, P., Smibert, P., Papalexi, E. & Satija, R. Integrating single-cell transcriptomic
736 data across different conditions, technologies, and species. *Nat. Biotechnol.* **36**, 411–420 (2018).
737 18. Harrow, J. *et al.* GENCODE: The reference human genome annotation for the ENCODE project.
738 *Genome Res.* **22**, 1760–1774 (2012).
739 19. Skelly, D. A. *et al.* Single-Cell Transcriptional Profiling Reveals Cellular Diversity and
740 Intercommunication in the Mouse Heart. *Cell Rep.* **22**, 600–610 (2018).
741 20. McLellan, M. A. *et al.* High-Resolution Transcriptomic Profiling of the Heart during Chronic Stress
742 Reveals Cellular Drivers of Cardiac Fibrosis and Hypertrophy. *Circulation* 1448–1463 (2020)
743 doi:10.1161/CIRCULATIONAHA.119.045115.
744 21. Mercer, T. R., Dinger, M. E., Sunkin, S. M., Mehler, M. F. & Mattick, J. S. Specific expression of
745 long noncoding RNAs in the mouse brain. *Proc. Natl. Acad. Sci. U. S. A.* **105**, 716–721 (2008).
746 22. Derrien, T. *et al.* The GENCODE v7 catalog of human long noncoding RNAs: Analysis of their
747 gene structure, evolution, and expression. *Genome Res.* **22**, 1775–1789 (2012).
748 23. Cabili, M. *et al.* Integrative annotation of human large intergenic noncoding RNAs reveals global
749 properties and specific subclasses. *Genes Dev.* **25**, 1915–1927 (2011).
750 24. Ulitsky, I. Evolution to the rescue: Using comparative genomics to understand long non-coding
751 RNAs. *Nat. Rev. Genet.* **17**, 601–614 (2016).
752 25. Piccoli, M.-T. *et al.* Inhibition of the Cardiac Fibroblast-Enriched lncRNA Meg3 Prevents Cardiac
753 Fibrosis and Diastolic Dysfunction. *Circ. Res.* CIRCRESAHA.117.310624 (2017)
754 doi:10.1161/CIRCRESAHA.117.310624.
755 26. Hofmann, P. *et al.* Long non-coding RNA H19 regulates endothelial cell aging via inhibition of
756 STAT3 signalling. *Cardiovasc. Res.* **115**, 230–242 (2019).
757 27. Han, P. *et al.* A long noncoding RNA protects the heart from pathological hypertrophy. *Nature*
758 **514**, 102–106 (2014).
759 28. Alexanian, M. & Haldar, S. M. The cardiac myofibroblast from supporting cast to leading role?
760 *Circ. Res.* **123**, 1258–1260 (2018).
761 29. Guttman, M. *et al.* Chromatin signature reveals over a thousand highly conserved large non-
762 coding RNAs in mammals. *Nature* **458**, 223–227 (2009).
763 30. Wucher, V. *et al.* FEELnc: A tool for long non-coding RNA annotation and its application to the
764 dog transcriptome. *Nucleic Acids Res.* **45**, 1–12 (2017).
765 31. Liu, F., Zhou, P., Wang, Q., Zhang, M. & Li, D. The Schlafen family: complex roles in different
766 cell types and virus replication. *Cell Biol. Int.* **42**, 2–8 (2018).
767 32. Hezroni, H. *et al.* Principles of Long Noncoding RNA Evolution Derived from Direct Comparison
768 of Transcriptomes in 17 Species. *Cell Rep.* **11**, 1110–1122 (2015).
769 33. Luo, Y. *et al.* New developments on the Encyclopedia of DNA Elements (ENCODE) data portal.
770 *Nucleic Acids Res.* **48**, D882–D889 (2020).
771 34. Avsec, Z., Barekatain, M., Cheng, J. & Gagneur, J. Modeling positional effects of regulatory
772 sequences with spline transformations increases prediction accuracy of deep neural networks.
773 *Bioinformatics* **34**, 1261–1269 (2018).

774 35. Van Nostrand, E. L. *et al.* Robust transcriptome-wide discovery of RNA-binding protein binding
775 sites with enhanced CLIP (eCLIP). *Nat. Methods* **13**, 508–514 (2016).
776 36. Dunham, I. *et al.* An integrated encyclopedia of DNA elements in the human genome. *Nature*
777 **489**, 57–74 (2012).
778 37. Shi, L., Shi, L., Wang, X. & He, J. Regulatory Roles of Osteopontin in Production of Monocyte-
779 Origin MCP-1. *Cell Transplant.* **27**, 1185–1194 (2018).
780 38. Gregory, J. L. *et al.* Macrophage Migration Inhibitory Factor Induces Macrophage Recruitment
781 via CC Chemokine Ligand 2. *J. Immunol.* **177**, 8072–8079 (2006).
782 39. Uhlén, M. *et al.* The human secretome. *Sci. Signal.* **12**, 1–9 (2019).
783 40. Redecke, V. *et al.* Hematopoietic progenitor cell lines with myeloid and lymphoid potential. *Nat.*
784 *Methods* **10**, 795–803 (2013).
785 41. Platt, R. J. *et al.* CRISPR-Cas9 knockin mice for genome editing and cancer modeling. *Cell* **159**,
786 440–455 (2014).
787 42. Marx, V. Method of the Year: spatially resolved transcriptomics. *Nat. Methods* **18**, 9–14 (2021).
788 43. Svensson, V. *et al.* Power analysis of single-cell rnA-sequencing experiments. *Nat. Methods* **14**,
789 381–387 (2017).
790 44. Rhee, A. J. & Lavine, K. J. New Approaches to Target Inflammation in Heart Failure: Harnessing
791 Insights from Studies of Immune Cell Diversity. *Annu. Rev. Physiol.* **82**, 1–20 (2020).
792 45. Duncan, S. E. *et al.* Macrophage Activities in Myocardial Infarction and Heart Failure. *Cardiol.*
793 *Res. Pract.* **2020**, (2020).
794 46. Moskalik, A., Niderla-Bielińska, J. & Ratajska, A. Multiple roles of cardiac macrophages in heart
795 homeostasis and failure. *Heart Fail. Rev.* (2021) doi:10.1007/s10741-021-10156-z.
796 47. Peet, C., Ivetic, A., Bromage, D. I. & Shah, A. M. Cardiac monocytes and macrophages after
797 myocardial infarction. *Cardiovasc. Res.* **116**, 1101–1112 (2020).
798 48. Liao, X. *et al.* Distinct roles of resident and nonresident macrophages in nonischemic
799 cardiomyopathy. *Proc. Natl. Acad. Sci. U. S. A.* **115**, E4661–E4669 (2018).
800 49. Leuschner, F. *et al.* Rapid monocyte kinetics in acute myocardial infarction are sustained by
801 extramedullary monocytopoiesis. *J. Exp. Med.* **209**, 123–137 (2012).
802 50. Dutta, P. *et al.* Myocardial infarction activates CCR2+ hematopoietic stem and progenitor cells.
803 *Cell Stem Cell* **16**, 477–487 (2015).
804 51. Dutta, P. *et al.* Myocardial infarction accelerates atherosclerosis. *Nature* **487**, 325–329 (2012).
805 52. Aoki, S. *et al.* Elevated peripheral blood mononuclear cell count is an independent predictor of
806 left ventricular remodeling in patients with acute myocardial infarction. *J. Cardiol.* **57**, 202–207
807 (2011).
808 53. Van Der Laan, A. M. *et al.* A proinflammatory monocyte response is associated with myocardial
809 injury and impaired functional outcome in patients with ST-segment elevation myocardial
810 infarction: Monocytes and myocardial infarction. *Am. Heart J.* **163**, 57-65.e2 (2012).
811 54. Swirski, F. K. & Al., E. Identification of Splenic Reservoir. *Science (80-.).* **325**, 612–616 (2009).
812 55. Frantz, S. & Nahrendorf, M. Cardiac macrophages and their role in ischaemic heart disease.
813 *Cardiovasc. Res.* **102**, 240–248 (2014).
814 56. Bajpai, G. *et al.* Tissue Resident CCR2- and CCR2+ Cardiac Macrophages Differentially

815 Orchestrate Monocyte Recruitment and Fate Specification Following Myocardial Injury. *Circ.*
816 *Res.* **124**, 263–278 (2019).
817 57. Yakar Tülüce, S. *et al.* Galectin-3 levels in patients with hypertrophic cardiomyopathy and its
818 relationship with left ventricular mass index and function. *Anatol. J. Cardiol.* **16**, 344–348 (2016).
819 58. Frunza, O. *et al.* Myocardial Galectin-3 Expression Is Associated with Remodeling of the
820 Pressure-Overloaded Heart and May Delay the Hypertrophic Response without Affecting
821 Survival, Dysfunction, and Cardiac Fibrosis. *Am. J. Pathol.* **186**, 1114–1127 (2016).
822 59. Danella Polli, C. *et al.* Monocyte Migration Driven by Galectin-3 Occurs through Distinct
823 Mechanisms Involving Selective Interactions with the Extracellular Matrix. *ISRN Inflamm.* **2013**,
824 1–9 (2013).
825 60. Jia, W., Kidoya, H., Yamakawa, D., Naito, H. & Takakura, N. Galectin-3 accelerates M2
826 macrophage infiltration and angiogenesis in tumors. *Am. J. Pathol.* **182**, 1821–1831 (2013).
827 61. Papaspyridonos, M. *et al.* Galectin-3 is an amplifier of inflammation in atherosclerotic plaque
828 progression through macrophage activation and monocyte chemoattraction. *Arterioscler.*
829 *Thromb. Vasc. Biol.* **28**, 433–440 (2008).
830 62. Ramanujam, D., Sassi, Y., Laggerbauer, B. & Engelhardt, S. Viral vector-based targeting of miR-
831 21 in cardiac nonmyocyte cells reduces pathologic remodeling of the heart. *Mol. Ther.* **24**, 1939–
832 1948 (2016).
833 63. Hwang, H. W., Wentzel, E. A. & Mendell, J. T. A hexanucleotide element directs microRNA
834 nuclear import. *Science (80-.).* **315**, 97–100 (2007).
835 64. Ziegler, C. *et al.* The long non-coding RNA LINC 00941 and SPRR 5 are novel regulators of
836 human epidermal homeostasis . *EMBO Rep.* **20**, 1–13 (2019).
837 65. Stuart, T. *et al.* Comprehensive Integration of Single-Cell Data. *Cell* **177**, 1888-1902.e21 (2019).
838 66. Hafemeister, C. & Satija, R. Normalization and variance stabilization of single-cell RNA-seq data
839 using regularized negative binomial regression. *Genome Biol.* **20**, 1–15 (2019).
840 67. Scrucca, L., Fop, M., Murphy, T. B. & Raftery, A. E. Mclust 5: Clustering, classification and
841 density estimation using Gaussian finite mixture models. *R J.* **8**, 289–317 (2016).
842 68. Linderman, G. C., Zhao, J. & Kluger, Y. Zero-preserving imputation of scRNA-seq data using
843 low-rank approximation. *bioRxiv* 397588 (2018) doi:10.1101/397588.
844 69. Sherman, B. T. *et al.* DAVID: a web server for functional enrichment analysis and functional
845 annotation of gene lists (2021 update). *Nucleic Acids Res.* 1–6 (2022) doi:10.1093/nar/gkac194.
846 70. Jin, S. *et al.* Inference and analysis of cell-cell communication using CellChat. *Nat. Commun.* **12**,
847 1–20 (2021).
848 71. Afgan, E. *et al.* The Galaxy platform for accessible, reproducible and collaborative biomedical
849 analyses: 2018 update. *Nucleic Acids Res.* **46**, W537–W544 (2018).
850 72. Dobin, A. *et al.* STAR: Ultrafast universal RNA-seq aligner. *Bioinformatics* **29**, 15–21 (2013).
851 73. Pertea, M. *et al.* StringTie enables improved reconstruction of a transcriptome from RNA-seq
852 reads. *Nat. Biotechnol.* **33**, 290–295 (2015).
853 74. Quinlan, A. R. & Hall, I. M. BEDTools: A flexible suite of utilities for comparing genomic features.
854 *Bioinformatics* **26**, 841–842 (2010).
855 75. Wang, L. *et al.* CPAT: Coding-potential assessment tool using an alignment-free logistic

856 regression model. *Nucleic Acids Res.* **41**, 1–7 (2013).
857 76. Love, M. I., Huber, W. & Anders, S. Moderated estimation of fold change and dispersion for RNA-
858 seq data with DESeq2. *Genome Biol.* **15**, 1–21 (2014).
859 77. Metsalu, T. & Vilo, J. ClustVis: A web tool for visualizing clustering of multivariate data using
860 Principal Component Analysis and heatmap. *Nucleic Acids Res.* **43**, W566–W570 (2015).
861 78. Bindea, G. *et al.* ClueGO: A Cytoscape plug-in to decipher functionally grouped gene ontology
862 and pathway annotation networks. *Bioinformatics* **25**, 1091–1093 (2009).
863 79. Shannon, P. *et al.* Cytoscape: A software Environment for integrated models of biomolecular
864 interaction networks. *Genome Res.* **13**, 2498–2504 (2003).
865 80. Avsec, Ž. *et al.* The Kipoi repository accelerates community exchange and reuse of predictive
866 models for genomics. *Nat. Biotechnol.* **37**, 592–600 (2019).
867

Figure 1

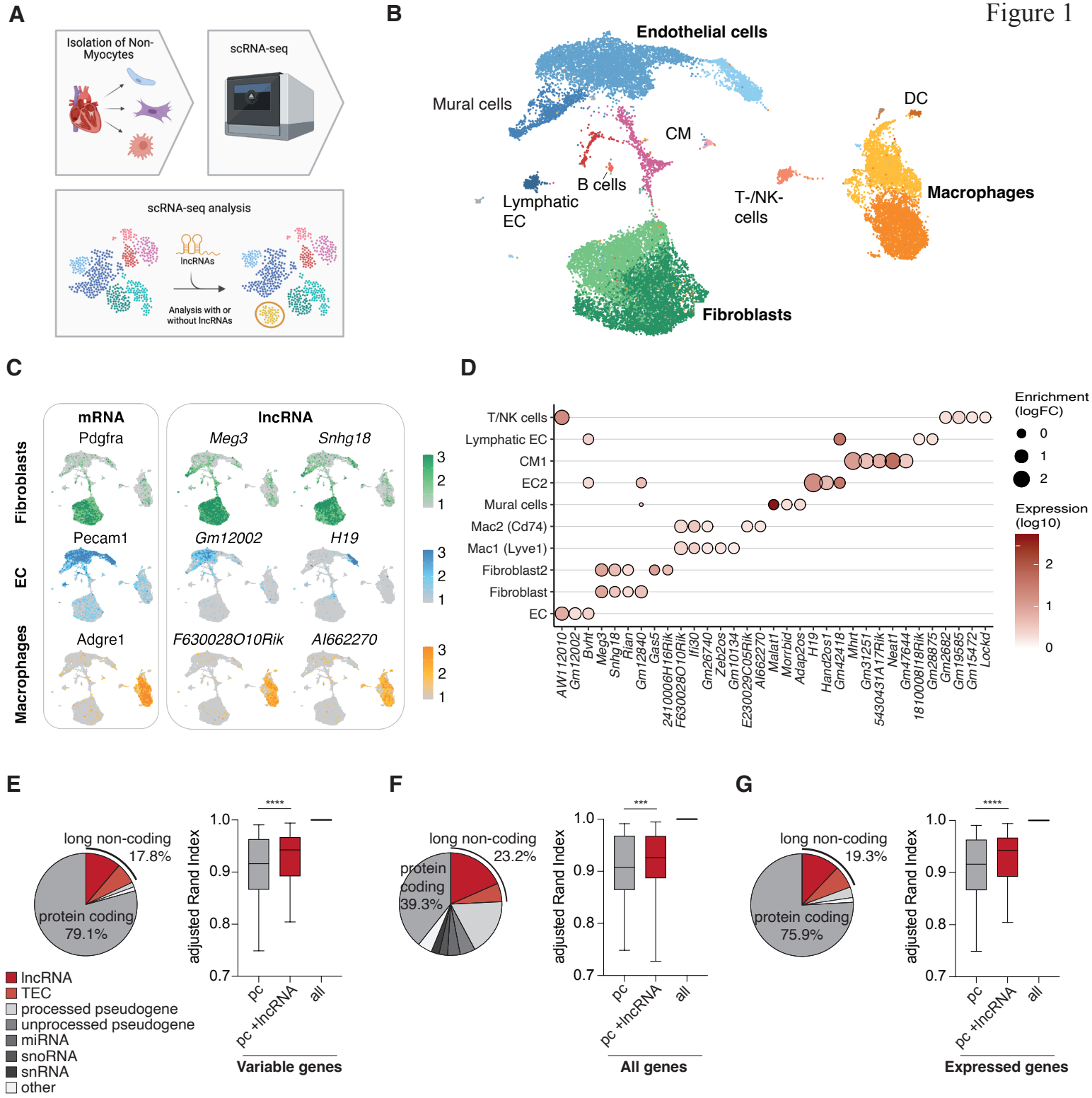
A
Isolation of Non-Myocytes
scRNA-seq
scRNA-seq analysis
lncRNAs
Analysis with or without lncRNAs
B
Endothelial cells
Mural cells
CM
DC
B cells
Lymphatic EC
T-/NK-cells
Macrophages
Fibroblasts
C
mRNA
lncRNA
Fibroblasts
EC
Macrophages
Pdgfra
Meg3
Snhg18
Pecam1
Gm12002
H19
Adgre1
F630028O10Rik
AI662270
D
T/NK cells
Lymphatic EC
CM1
EC2
Mural cells
Mac2 (Cd74)
Mac1 (Lyve1)
Fibroblast2
Fibroblast
EC
Enrichment (logFC)
Expression (log10)
E
long non-coding 17.8%
protein coding 79.1%
lncRNA
TEC
processed pseudogene
unprocessed pseudogene
miRNA
snoRNA
snRNA
other
adjusted Rand Index
pc
pc +lncRNA
all
Variable genes
F
long non-coding 23.2%
protein coding 39.3%
All genes
G
long non-coding 19.3%
protein coding 75.9%
Expressed genes
H
Cluster
No separate cluster
Venous capillary ECs
Pericytes
Fabp4+ Macs
Notch2+ fibroblast
protein coding + lncRNA
protein coding

Figure 1: LncRNA are important determinants for definition of specific cell types.

(A) Illustration for the measurement of lncRNA in murine myocardium and re-clustering analysis. (B) UMAP projection of murine myocardium as measured by single-cell sequencing (scRNA-seq). Cell populations are colored by type as indicated by the label. DC: dendritic cells, EC: endothelial cells, CM: cardiac myocytes. (C) Bubble plot showing lncRNA marker genes conserved across conditions. Bubble size corresponds to enrichment (logFC) and fill color to expression value (log10). Only values/bubbles with a significant enrichment (p-val < 0.05) are shown. (D) Feature plots showing mRNA and lncRNA markers for fibroblasts, endothelial cells (EC) and macrophages. (E), (F), (G) Adjusted Rand Index (ARI) calculation. In order to compare the clusterings with and without lncRNAs, the respective complete gene set was considered to yield the optimal clustering. We iterated the clustering in 0.01 steps with resolutions ranging from 0.10 to 1.00, testing for the similarity to optimal clustering using adjusted Rand index scoring. Here, the more similar a clustering would be to the "optimal" one the closer it will be to 1. (E) ARI calculation for the top variable genes (3,000 genes). (F) ARI calculation for all annotated genes (Gencode vM22 [18]). (G) ARI calculation for all expressed genes (expression value >0). pc: protein coding (H) Umap projection of murine myocardium with cell population clustering based on protein coding genes plus lncRNA genes (left panel) or only protein coding genes (right panel). The middle panel shows differentially assigned cell population clusters.

Figure 2

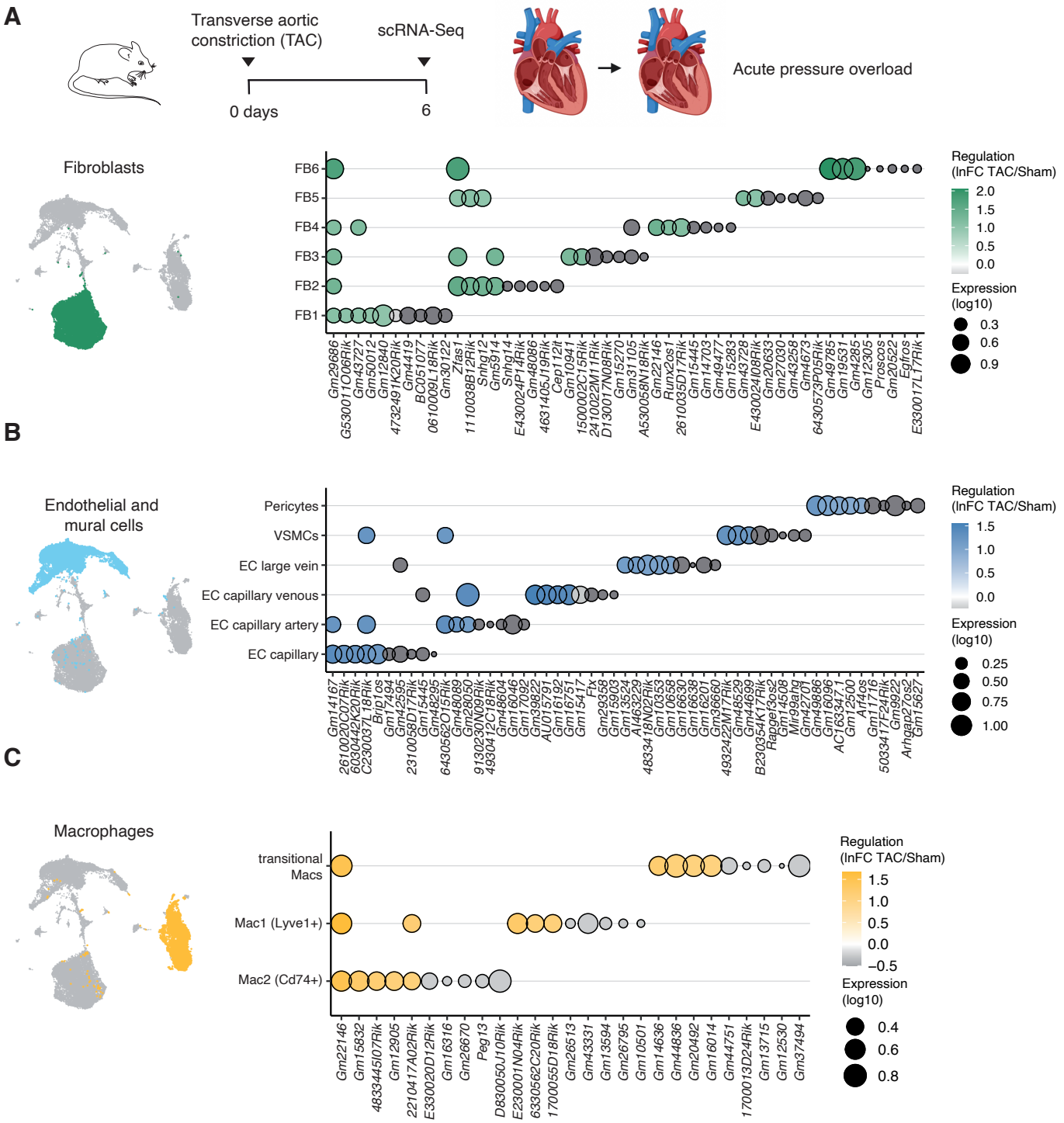
A
Transverse aortic constriction (TAC)
scRNA-Seq
0 days
6
Acute pressure overload
Fibroblasts
FB6
FB5
FB4
FB3
FB2
FB1
Gm29686
G530011O06Rik
Gm43727
Gm50012
Gm12840
4732491K20Rik
Gm4419
BC051077
0610009L18Rik
Gm30122
Zfas1
1110038B12Rik
Snhg12
Gm5914
Snhg14
E430024P14Rik
Gm48086
4631405J19Rik
Cep112it
Gm10941
1500002C15Rik
2410022M11Rik
D130017N08Rik
Gm15270
Gm31105
A530058N18Rik
Gm22146
Runx2os1
2610035D17Rik
Gm15445
Gm14703
Gm49477
Gm15283
Gm43728
E430024I08Rik
Gm20633
Gm27030
Gm43258
Gm4673
6430573P05Rik
Gm49785
Gm19531
Gm4285
Gm12305
Proscos
Gm20522
Eqtros
E330017L17Rik
Regulation (lnFC TAC/Sham)
2.0
1.5
1.0
0.5
0.0
Expression (log10)
0.3
0.6
0.9
B
Endothelial and mural cells
Pericytes
VSMCs
EC large vein
EC capillary venous
EC capillary artery
EC capillary
Gm14167
2610020C07Rik
6030442K20Rik
C230037L18Rik
Brip1os
Gm17494
Gm42595
2310058D17Rik
Gm15445
Gm48295
6430562O15Rik
Gm48089
Gm28050
9130230N09Rik
4930412C18Rik
Gm48604
Gm16046
Gm17092
Gm39822
AU015791
Gm16192
Gm16751
Gm15417
Fx
Gm29368
Gm15903
Gm13524
A1463229
4833418N02Rik
Gm10353
Gm10658
Gm16630
Gm16638
Gm16201
Gm36660
4932422M17Rik
Gm48529
Gm44699
B230354K17Rik
Rapgef3os2
Gm14508
Mir99ahg
Gm42701
Gm49886
Gm16096
AC163347.1
Gm12500
Ar4os
Gm11716
5033417F24Rik
Gm9922
Arhgap25os2
Gm15627
Regulation (lnFC TAC/Sham)
1.5
1.0
0.5
0.0
Expression (log10)
0.25
0.50
0.75
1.00
C
Macrophages
transitional Macs
Mac1 (Lyve1+)
Mac2 (Cd74+)
Gm22146
Gm15832
4833445I07Rik
Gm12905
2210417A02Rik
E330020D12Rik
Gm16316
Gm26670
Peg13
D830050J10Rik
E230001N04Rik
6330562C20Rik
1700055D18Rik
Gm26513
Gm43331
Gm13594
Gm26795
Gm10501
Gm14636
Gm44836
Gm20492
Gm16014
Gm44751
1700013D24Rik
Gm13715
Gm12530
Gm37494
Regulation (lnFC TAC/Sham)
1.5
1.0
0.5
0.0
−0.5
Expression (log10)
0.4
0.6
0.8

Figure 2: Dynamic changes of lncRNA expression in crMPs during pressure overload.

Bubble plot showing the top 5 up-regulated and top 5 down-regulated lncRNA genes after TAC for the sub-populations of the major cell types in the heart: (A) Fibroblasts (B) Endothelial cells and (C) Macrophages. Fill color corresponds to regulation in TAC vs. sham (lnFC TAC/sham) and bubble size corresponds to expression value (log10). Only values with a significant enrichment (p-val < 0.05) are shown. Some genes are among the top regulated genes in more than one cell type.

Figure 3

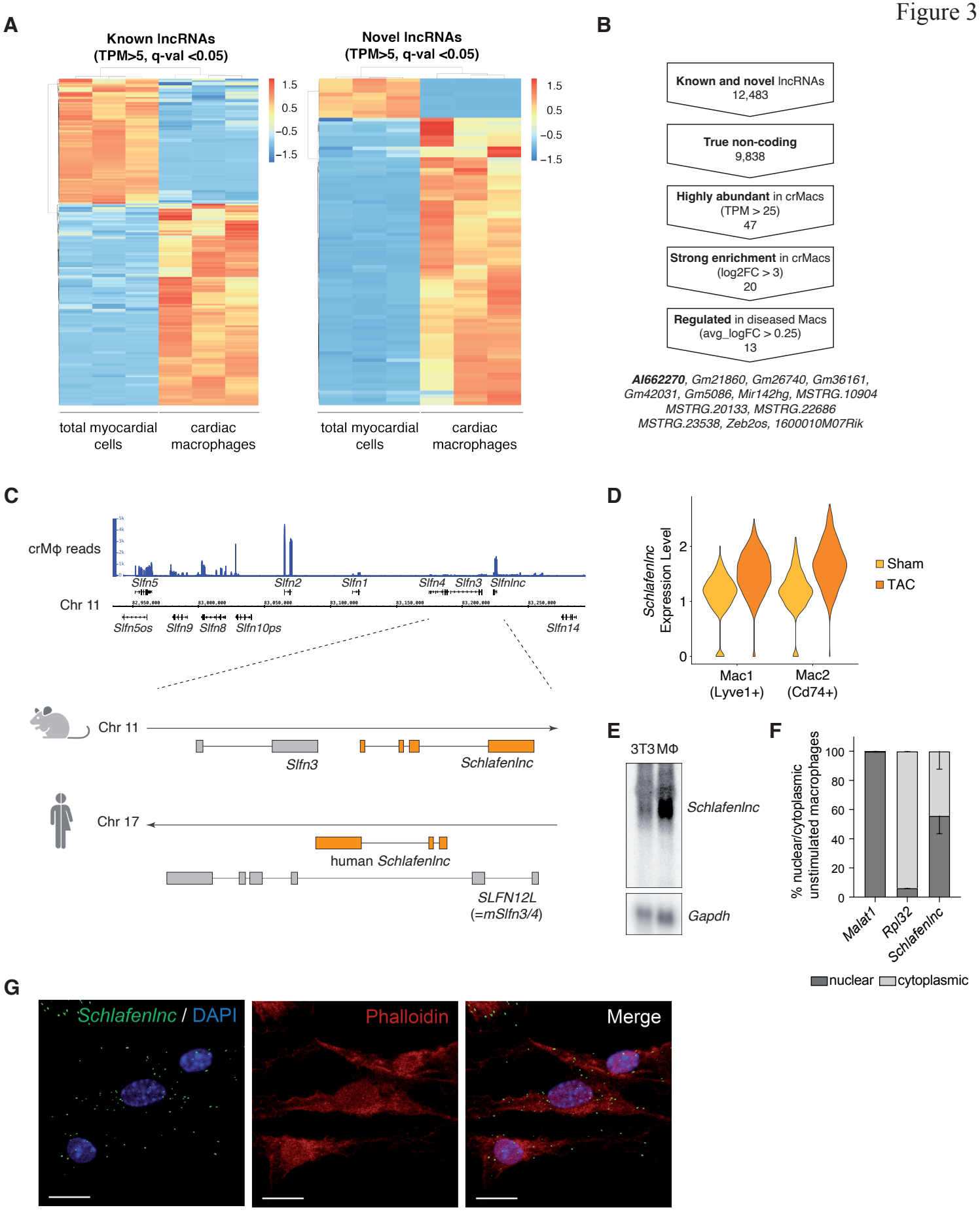
A
Known lncRNAs
(TPM>5, q-val <0.05)
Novel lncRNAs
(TPM>5, q-val <0.05)
1.5
0.5
−0.5
−1.5
total myocardial cells
cardiac macrophages
B
Known and novel lncRNAs
12,483
True non-coding
9,838
Highly abundant in crMacs
(TPM > 25)
47
Strong enrichment in crMacs
(log2FC > 3)
20
Regulated in diseased Macs
(avg_logFC > 0.25)
13
AI662270, Gm21860, Gm26740, Gm36161,
Gm42031, Gm5086, Mir142hg, MSTRG.10904
MSTRG.20133, MSTRG.22686
MSTRG.23538, Zeb2os, 1600010M07Rik
C
crMϕ reads
Chr 11
Slfn5
Slfn2
Slfn1
Slfn4
Slfn3
Slfnlnc
Slfn5os
Slfn9
Slfn8
Slfn10ps
Slfn14
Chr 11
Slfn3
Schlafenlnc
Chr 17
human Schlafenlnc
SLFN12L
(=mSlfn3/4)
D
Schlafenlnc
Expression Level
Sham
TAC
Mac1
(Lyve1+)
Mac2
(Cd74+)
E
3T3 MΦ
Schlafenlnc
Gapdh
F
% nuclear/cytoplasmic
unstimulated macrophages
Malat1
Rpl32
Schlafenlnc
nuclear
cytoplasmic
G
Schlafenlnc / DAPI
Phalloidin
Merge

Figure 3: Determination and annotation of the lncRNA landscape of cardiac resident macrophages.

(A) Unsupervised clustering of known and novel lncRNAs using normalized counts values, rows were averaged across samples for clustering. Genes shown are expressed with a TPM value >5 and differentially regulated (enriched) with a q-val of <0.05. (B) Flow scheme for the identification of lncRNA candidates using the indicated filters. (C) The Schlafen family locus showing the expression in cardiac resident macrophages (accumulated plus and minus strand). Lower panel: Zoom in of the *Schlafenlnc* locus in mouse as well as human for comparison. (D) Expression of the lncRNA *Schlafenlnc* in Mac1 (*Lyve1*+ macrophages) and Mac2 (MHCII high, *Cd74*+ macrophages) after sham or TAC in the scRNA-seq data. (E) Northern Blot showing the expression of *Schlafenlnc* transcripts in bone marrow-derived macrophages in comparison to fibroblasts (NIH3T3 cell line). (F) Relative nuclear and cytoplasmic localization of *Malat1* (nuclear lncRNA), *Rpl32* (mRNA) and *Schlafenlnc* as determined by fractionation of macrophages followed by quantification through RNA-Seq. (G) Detection of *Schlafenlnc* (green) in macrophages by RNA *in situ* hybridization (RNAScope). Nuclei were stained with DAPI (blue), Phalloidin (red) was used for outlining the cellular body (Scale bars = 15µm).

Figure 4

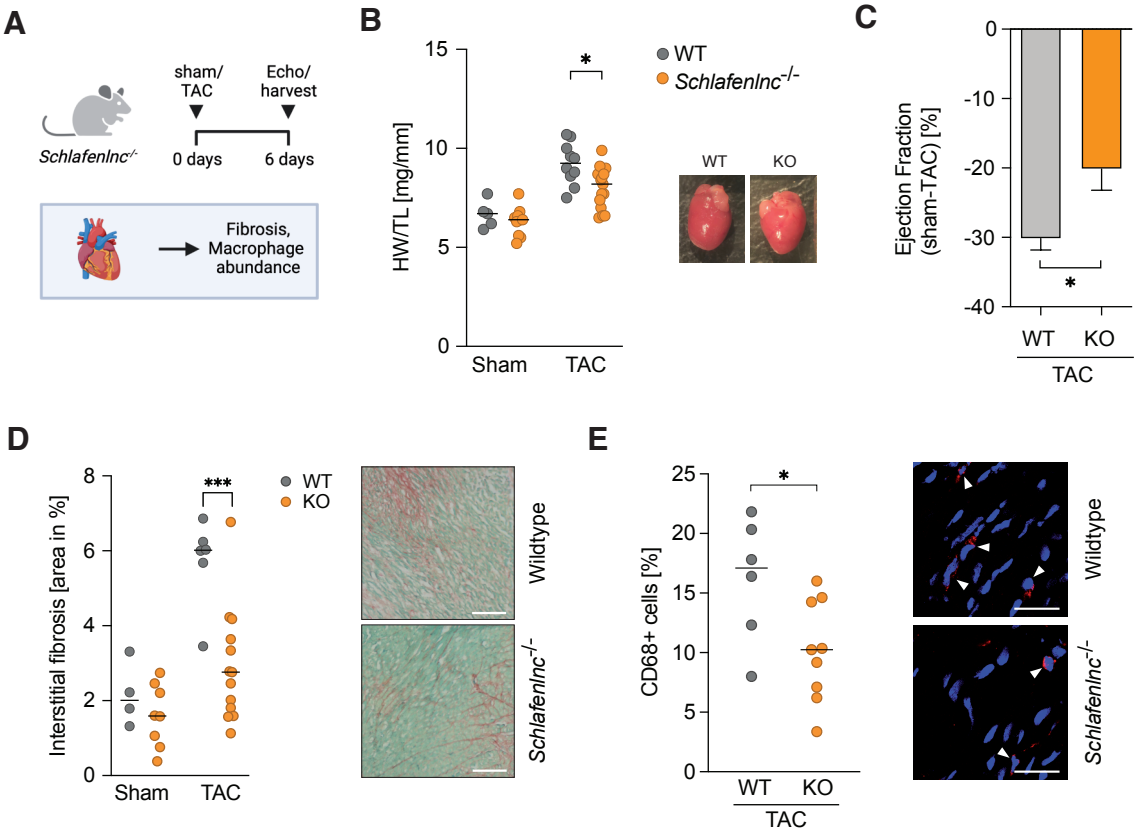
A
sham/ TAC
Echo/ harvest
SchlafenInc-/-
0 days
6 days
Fibrosis, Macrophage abundance
B
HW/TL [mg/mm]
15
10
5
0
Sham
TAC
*
WT
SchlafenInc-/-
WT
KO
C
Ejection Fraction (sham-TAC) [%]
0
-10
-20
-30
-40
*
WT
KO
TAC
D
Interstitial fibrosis [area in %]
8
6
4
2
0
Sham
TAC
***
WT
KO
Wildtype
SchlafenInc-/-
E
CD68+ cells [%]
25
20
15
10
5
0
*
WT
KO
TAC
Wildtype
SchlafenInc-/-

Figure 4: *SchlafenInc*-deficient mice show improved cardiac function and reduced inflammatory response after transverse aortic constriction (TAC).

(A) Experimental setup of cardiac phenotyping of *SchlafenInc*$^{-/-}$ and wildtype mice. (B) Quantification of normalized heart weight after TAC. HW= heart weight, TL= tibia length. C) Ejection fraction changes after 6 days TAC. (C) Left: Quantification of interstitial fibrosis by Sirius red/Fast green staining. Right: Representative images of interstitial fibrosis, scale bar = 200µm. (D) Representative images and quantification of macrophage/monocyte content by Cd68 staining in WT and *SchlafenInc*$^{-/-}$ hearts after 6d after TAC. White arrows label Cd68-positive cells, scale bar = 25µm.

Figure 5

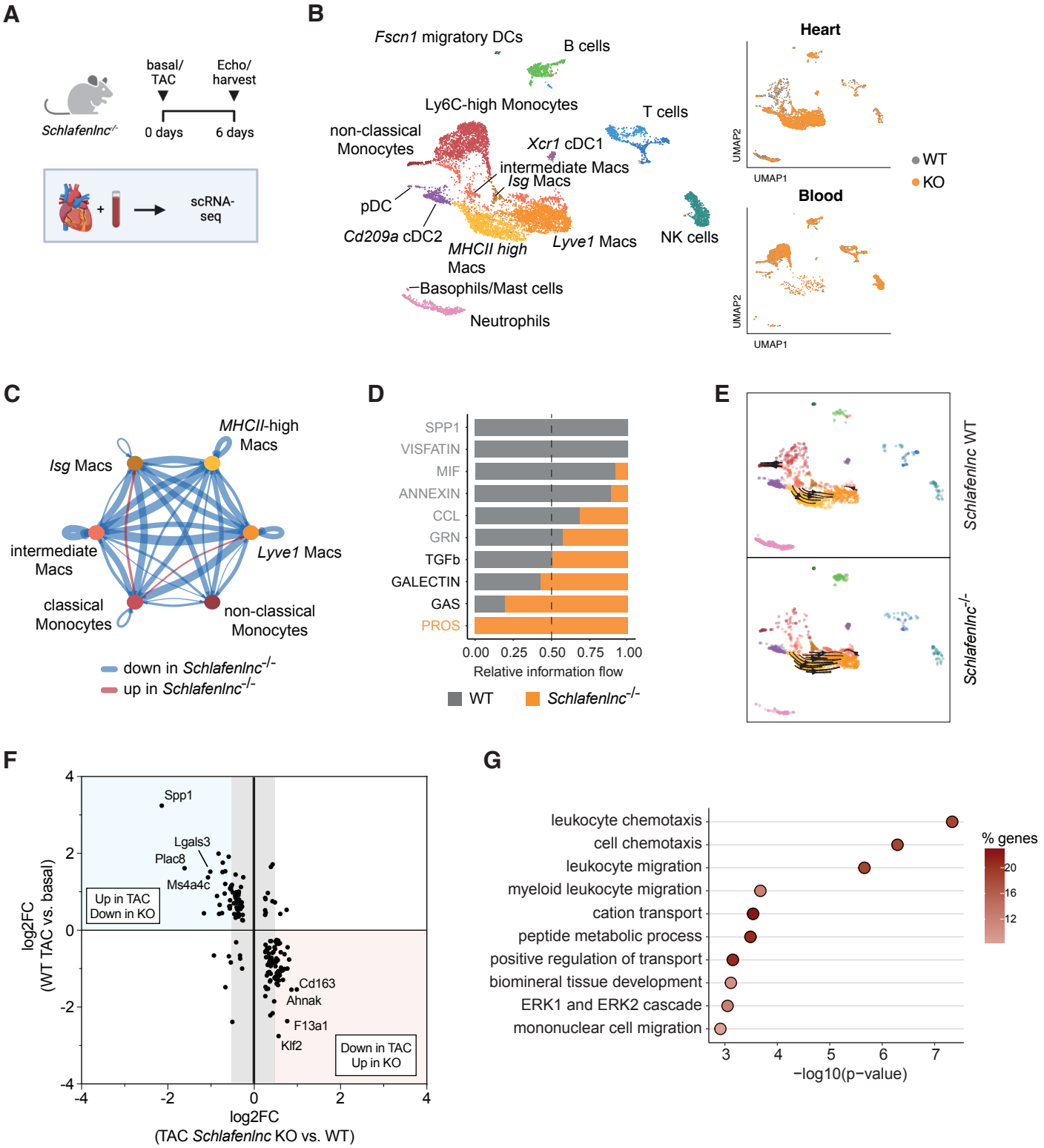
A
basal/ TAC
Echo/ harvest
Schlafenlnc-/-
0 days
6 days
scRNA-seq
B
Fscn1 migratory DCs
B cells
Ly6C-high Monocytes
T cells
non-classical Monocytes
Xcr1 cDC1
intermediate Macs
Isg Macs
pDC
Cd209a cDC2
MHCII high Macs
Lyve1 Macs
NK cells
Basophils/Mast cells
Neutrophils
Heart
Blood
UMAP1
UMAP2
WT
KO
C
MHCII-high Macs
Isg Macs
intermediate Macs
Lyve1 Macs
classical Monocytes
non-classical Monocytes
down in Schlafenlnc-/-
up in Schlafenlnc-/-
D
SPP1
VISFATIN
MIF
ANNEXIN
CCL
GRN
TGFb
GALECTIN
GAS
PROS
0.00 0.25 0.50 0.75 1.00
Relative information flow
WT
Schlafenlnc-/-
E
Schlafenlnc WT
Schlafenlnc-/-
F
Spp1
Lgals3
Plac8
Ms4a4c
Up in TAC Down in KO
Cd163
Ahnak
F13a1
Klf2
Down in TAC Up in KO
log2FC (WT TAC vs. basal)
log2FC (TAC Schlafenlnc KO vs. WT)
G
leukocyte chemotaxis
cell chemotaxis
leukocyte migration
myeloid leukocyte migration
cation transport
peptide metabolic process
positive regulation of transport
biomineral tissue development
ERK1 and ERK2 cascade
mononuclear cell migration
−log10(p−value)
% genes

Figure 5: scRNA-seq of *SchlafenInc*$^{-/-}$ mice reveals macrophage polarization towards an anti-inflammatory phenotype after TAC.

(A) Experimental setup of scRNA-seq of *SchlafenInc*$^{-/-}$ and wildtype mice. (B) Dimensional reduction (Umap) representation of combined measured cells with assigned cell types. (C) Cell interaction analysis of *SchlafenInc* WT and KO mice (CD45+ cells from blood and heart) after TAC using CellChat[70]. (D) Differential signaling in *SchlafenInc*$^{-/-}$ and WT macrophage and monocyte populations after TAC. (E) RNA Velocity of *SchlafenInc*$^{-/-}$ and WT cells from heart after 6 days of TAC. (F) Comparison of de-regulated genes (q-val<0.05) in TAC vs. basal condition in WT compared to de-regulated genes after 6d TAC KO vs. WT in *Lyve1*$^{+}$ macrophages (G) Gene ontology terms of genes de-regulated in *SchlafenInc*-deficient mice and after 6 days TAC.

Figure 6

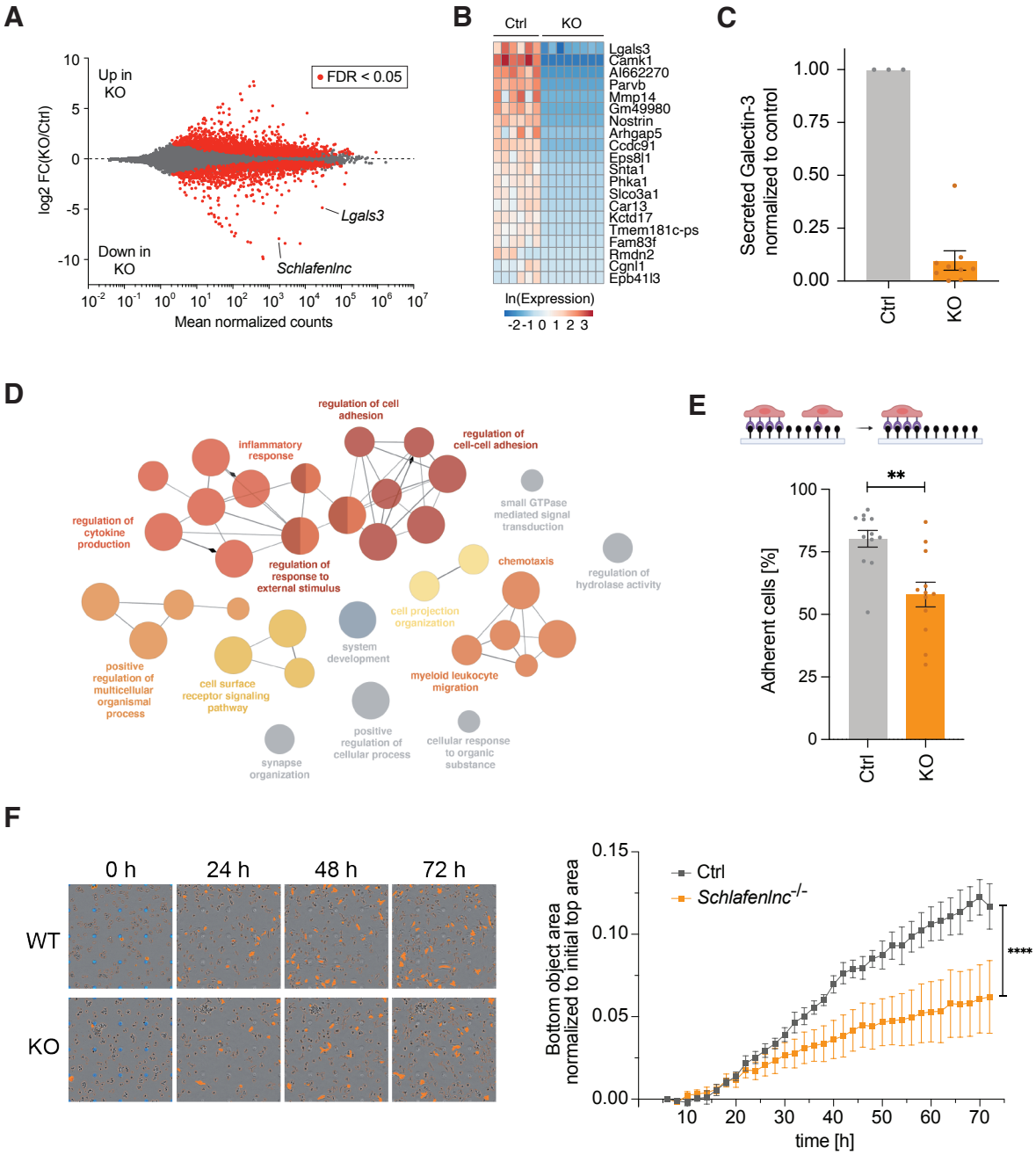
A
Up in KO
FDR < 0.05
Down in KO
Lgals3
SchlafenInc
log2 FC(KO/Ctrl)
Mean normalized counts
B
Ctrl
KO
Lgals3
Camk1
AI662270
Parvb
Mmp14
Gm49980
Nostrin
Arhgap5
Ccdc91
Eps8l1
Shta1
Phka1
Slco3a1
Car13
Kctd17
Tmem181c-ps
Fam83f
Rmdn2
Cgnl1
Epb41l3
ln(Expression)
C
Secreted Galectin-3 normalized to control
Ctrl
KO
D
regulation of cell adhesion
inflammatory response
regulation of cell-cell adhesion
small GTPase mediated signal transduction
regulation of cytokine production
regulation of response to external stimulus
chemotaxis
regulation of hydrolase activity
cell projection organization
system development
positive regulation of multicellular organismal process
cell surface receptor signaling pathway
myeloid leukocyte migration
positive regulation of cellular process
cellular response to organic substance
synapse organization
E
Adherent cells [%]
Ctrl
KO
F
0 h
24 h
48 h
72 h
WT
KO
Ctrl
SchlafenInc-/-
Bottom object area normalized to initial top area
time [h]

Figure 6: *SchlafenInc* is required for the activation of macrophage gene programs for cell adhesion and migration.

(A) MA plot showing differentially expressed genes in *SchlafenInc*$^{-/-}$ vs. Ctrl macrophages. Significantly deregulated genes (FDR < 0.05) are shown in red. (B) Heatmap of an unsupervised clustering showing the top 20 downregulated genes in *SchlafenInc*$^{-/-}$ macrophages. (C) Measurement of Galectin-3 protein secretion by control and *SchlafenInc*$^{-/-}$ macrophages as determined by ELISA. The supernatant of one control cell line and three *SchlafenInc*$^{-/-}$ clones were used in n=3 independent experiments. (D) Functionally grouped gene ontology term analysis of biological processes associated with significantly downregulated genes (FDR < 0.05, log2FC < -1) in *SchlafenInc*$^{-/-}$ macrophages. (E) Adhesion assay with control and *SchlafenInc*$^{-/-}$ macrophages (Ctrl clones n=2, KO clones n=3; 4 independent experiments). (F) Chemotaxis assay against a gradient of the chemokine C5a with control and *SchlafenInc*$^{-/-}$ macrophages stimulated with 10ng/ml LPS overnight (Ctrl clones n=1, KO clones n=3; 3 independent experiments).